Surface Texturing of Fan-blade Body by Random-orbital Polishing With in-line Aqueous Mist

Edgar Jeevan Danaraj
Advanced Remanufacturing and Technology Centre, Singapore
Swee Hock Yeo (mshyeo@ntu.edu.sg)
Nanyang Technological University https://orcid.org/0000-0003-1609-768X

Research Article

Keywords: Random-orbital Polishing, Finishing, Surface Roughness, Airfoil, Fan Blade

Posted Date: March 18th, 2021

DOI: https://doi.org/10.21203/rs.3.rs-309093/v1

Version of Record: A version of this preprint was published at The International Journal of Advanced Manufacturing Technology on August 21st, 2021. See the published version at https://doi.org/10.1007/s00170-021-07877-8.

Surface texturing of fan-blade body by random-orbital polishing with in-line aqueous mist

Edgar Jeevan Danaraj[1], Swee Hock Yeo[2, *]

[1] Advanced Remanufacturing and Technology Centre, Singapore
[2] School of Mechanical and Aerospace Engineering, Nanyang Technological University, Singapore 639798
*Email: mshyeo@ntu.edu.sg

Abstract

Airfoil structures such as fan blades have free form geometry which require a high level of precision in order to create a uniform finish for ideal gas path flow. Challenges in machining of such parts have led to rework in order to remove defects and conform to dimensional requirements at the same time. Mechanical polishing is the most common method to remove surface irregularities on fan blades such as scallop height, while maintaining the required dimensions. After the polishing process, the part will undergo shot peening, vibratory finishing and later, painting and coating at the final stages. It is therefore essential for the fan blade surface to pre-treated with rough, uniform textures in order to promote good surface-to-surface adhesion at the end of the manufacturing cycle.

Generally, the polishing process is assisted by an external cooling medium applied on the part surface at intervals. This method of removing heat is not effective, as the polished surface may experience scratches or distortion, especially around thin-walled sections of the leading edge in fan blade. The existing polishing method uses a single-axis rotary tool can produce average surface roughness, *Ra*, of 1.2 µm that satisfies the requirement. However, this form of aggressive polishing has a high material removal rate, resulting in excessive reduction in material thickness which leads to the rejection of costly fan blade.

This study a new localized polishing method and examines its effect on the surface topography of an airfoil component made of aluminum alloy. The area of interest is focused on the leading edge of a fan blade at which polishing is carried out using a random-orbital polishing tool with modified features to incorporate internal cooling capability. Experimental trials are conducted to study the effects of surface finish with fixed grain abrasive disks under four conditions. A cold gun is connected in-line to guide cold air inside the internal passages of the tool and out onto the surface of the part directly. A secondary cooling source by water nozzle spray is integrated in the tool to mix with the cold air jet and form an aerosol mist during tool activation.

Surface topography of the samples are determined by arithmetic mean deviation, maximum height and root mean square of the profile. Surface roughness was performed using an optical profilometer. The localized polishing method achieved a desirable surface roughness, *Ra* of 0.8 µm, while removing all traces of scallop height and maintaining the leading-edge thickness within tolerance. The study showed that the new method produced a topography that is uniformly textured. This method can improve the manufacturing cycle time.

Keywords Random-orbital Polishing; Finishing; Surface Roughness; Airfoil; Fan Blade

1. Introduction

Aluminum alloy 7255 has been used in many aerospace applications requiring high level of mechanical strength and good damage tolerance. Machining aluminum alloy fan blade is difficult to obtain uniform surface roughness because of the free form surfaces and thin structural requirements. A poor machining strategy will produce defects such as scallop heights on the fan blade surfaces. Surface peaks are sharp and considered as stress concentration where cracks may be initiated and subsequently propagate, causing fatigue failure – which is non-compliance in airworthiness standards in fan blades in aero engines. Therefore, surface defects must be removed, typically by mechanical polishing while attaining the target roughness value according to engineering specifications.

Surface topography of the roughness value is usually based on the *Ra* parameter. Axinte et al. [1] used belt polishing for final finishing of components to improve dimensional precision and surface quality. Xiao et al. [2] developed a similar abrasive belt polishing method for blades to achieve the desired surface properties. Mechanical polishing may either be in dry or wet condition for cooling of parts by removing heat generated in the abrasive process. Wu D. et al. [3] used flexible abrasive cloth wheel to polish titanium alloy blades in dry condition. The results showed that unevenness, and other defects of the blade surface are effectively removed and the dry method effectively improved the surface quality without exceeding the dimensional limits of the workpiece. The surface roughness was reduced from *Ra* of 1.2 µm to less than 0.40 µm.

Surface roughness is influenced by the properties of friction and wear of solid abrasives lubricated by water. When deionized water is applied to the abrasive material, slurry is formed, corresponding to the abrasive mechanism in chemical mechanical polishing. The relative movement of the slurry drawn between the polished surface and the pad creates the material removal mechanism [4]. In some studies, the effect of dry and wet polishing showed that polishing without water increased the surface roughness of the samples because the abrasive grains detached from the polishing tool may embed into the workpiece surface [5]. Wong et al. [6] investigated the effect of surface roughness on frictional characteristics in deionized water. It was discovered that the friction coefficient and surface roughness decreased with sliding distance in the materials tested with deionized water.

The effects of impinging air jets by compressed cold air have been studied by Choi [7]. It was reported that the effectiveness of the cold air in reducing thermal defects was almost similar to that with regular coolant with negligible material loss. The formation of tensile stresses in the surface was more evident and surface roughness would rise as the depth of cut increases. It was found that the lack of coolant in using dry cold air was almost certainly the main reason for this phenomenon to occur. The application of cold air showed some improvements compared with dry polishing. However, many important points of surface characterization have not been closely examined [8].

Saberi et al. [9] used a grinding technique called minimum quantity lubrication (MQL) technique by compressed cold air jet from a cold gun (vortex tube principle). This technique involved spraying a mixture of air and oil mist onto the cutting zone directly. MQL improved cooling and lubrication performance through the use of a cold gun which generated conditioned air at lower temperatures than ambient. The study of cooling effect with minimum quantity lubrication with air jet of 0.4 MPa pressure and 14°C temperature concluded that surface quality improved when compared to dry condition. Because of this reason, a condition has been set aside in this study to deploy the MQL technique and verify its combined effect (condition 4: air and water mist).

Use of pure air is another alternative but it has relatively poor cooling ability which may lead to low specific heat and low heat conductivity. Due to low mass flow rate of air streams (measured at 1.0 m/s) exiting the holes in the abrasive disk, the heat transfer coefficient will be smaller, regardless of its low temperature.

Design configuration of the abrasive end effector vary from circular wheels or belt types to cylindrical or conical grinding heads. For the circular type of wheels (round-shaped disk), a foam or inflatable backing pad may be used for flexibility on the free form geometry [10]. Axinte et al. [11] demonstrated that combining dual finishing methods (belt and bob) as a hybrid process would be beneficial for components with complex geometries, removing both machining marks and achieving required surface roughness to some extent. Zhao et al. [12] optimized the key process parameters for polishing of aero-engine blades to reduce the surface roughness and improve quality of the finish.

The existing polishing method of working on fan blade defects was carried out using a single-axis rotary tool. This type of tool has a singular rotational movement where the abrasive pad spins primarily around its axis. The challenge of using such a polishing tool is the generation of lay in the surface texture which would fail quality inspection. The other challenge for the rotary tool is high rate of material removal which would cause an undersized edge thickness of the fan blade. Lowering the cutting speed for this tool would be a possible option, but this may lead to defects such as particle embedment and uneven surface.

In this paper a new polishing tool is designed with random-orbital motion is introduced. Random-orbital tools move in two directions as opposed to one direction. This tool uses a mechanism that causes the disk to simultaneously rotate in a circle and oscillate in an eccentric pattern inside the circle to generate the vibration amplitude. Therefore, the mechanical action of the abrasive by random orbit is vibratory motion instead of fixed rotation.

2. Experimental methodology

2.1 Experimental conditions

Direct bolt-on modification is done to implement in-line air- and water-cooling features for the random-orbital tool. The main body of the tool requires a replacement of the shroud assembly from a different housing model. This would allow the supply of air to flow directly through the internal passages of the tool and abrasive disk, and out onto the workpiece surface.

For the existing single-axis rotary method, an angle grinder, Toku model TAG400 was used for comparison. The pressure was fixed at 620 kPa and the speed was set at 10,000 rpm. For the existing method shown in figure 1(a), a plastic squeeze bottle was used to spray deionized water on the surface for spot cooling, at 3-minute intervals over a total process time of 9 minutes. Due to the external spot cooling from the single nozzle of the bottle, the heat affected zone is not targeted directly. This method has minimal cooling effectiveness as a result. The new method proposed for the experiments uses a palm-style wet Dynorbital® tool (model number 57583). Figure 1(b) shows a modified version of the random-orbital tool which includes a water spray nozzle mounted forward-facing, at approximately 45° angle through the main body.

The deionized water was supplied to the tool by a centralized distillation system that feeds the water utility equipment at the polishing booth. Utilizing deionized water as a wetting medium is to cool the workpiece surface and formulate a slurry during polishing process. An integral water spray valve was installed in the shroud near the free-floating spindle as shown in figure 1(c). The chemical-mechanical reaction of the wet abrasives is expected to breakdown into fine particles and form a slurry, depending on the amount of water and force applied. For the wet condition combined with cold air, the temperature of the water would be further lowered for more effective heat dissipation.

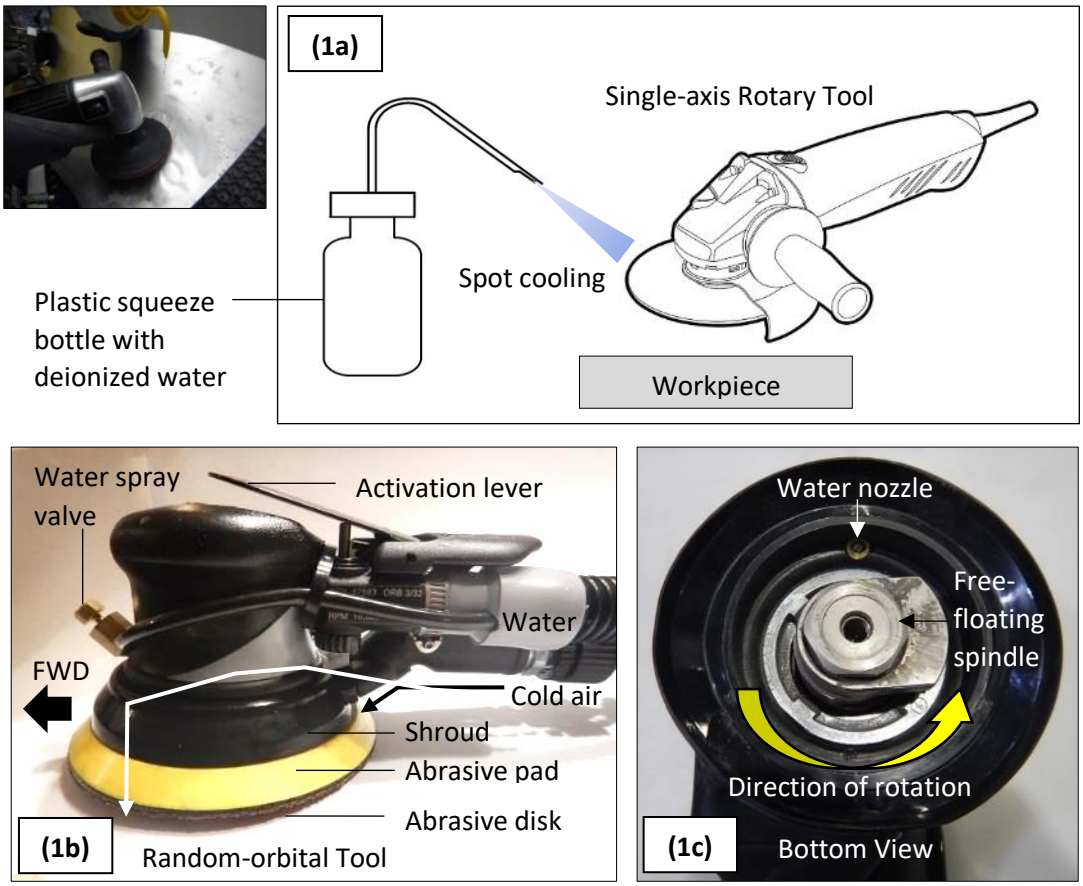

Figure 1. (a) Existing method by single-axis rotary tool with external spot cooling with a plastic bottled water, (b) Modified design of the random-orbital tool with integral cold air (indicated by the black arrow) and water (indicated by the white arrow), and (c) Free-floating spindle and water nozzle location (viewed from the bottom of the shroud with abrasive disk and pad removed).

The random-orbital tool was fitted with an air shroud of a different model initially intended for vacuum dust extraction. However, the purpose of this is to feed air through the internals of the tool and escape out of the abrasive disk holes. A cold gun was connected in-line to the port of the shroud by a flexible hose for the air coolant supply. As shown in figure 2, the cold gun module generates two streams at different temperature from a single compressed injection. The cold gun separates the compressed air into two opposite directions, where hot air is exhausted from the rear end and forcing the cold air at the front end due to the lowered pressure gradient at the cold section [13]. A standard cold gun system (ExAir model 5215) with a single outlet is used. This enabled the random-orbital tool to flow multiple streams of cold air out of the holes in the disk as shown in figure 1(a). By adjusting the incoming air pressure at the regulator (620 kPa), the cold gun maintained an air pressure of 300 kPa in-line, and 172 kPa at the outlet port to the tube. The rate of cold air flow escaping out if the abrasive disk holes in running operation was measured at 1.0 m/s using a standard anemometer.

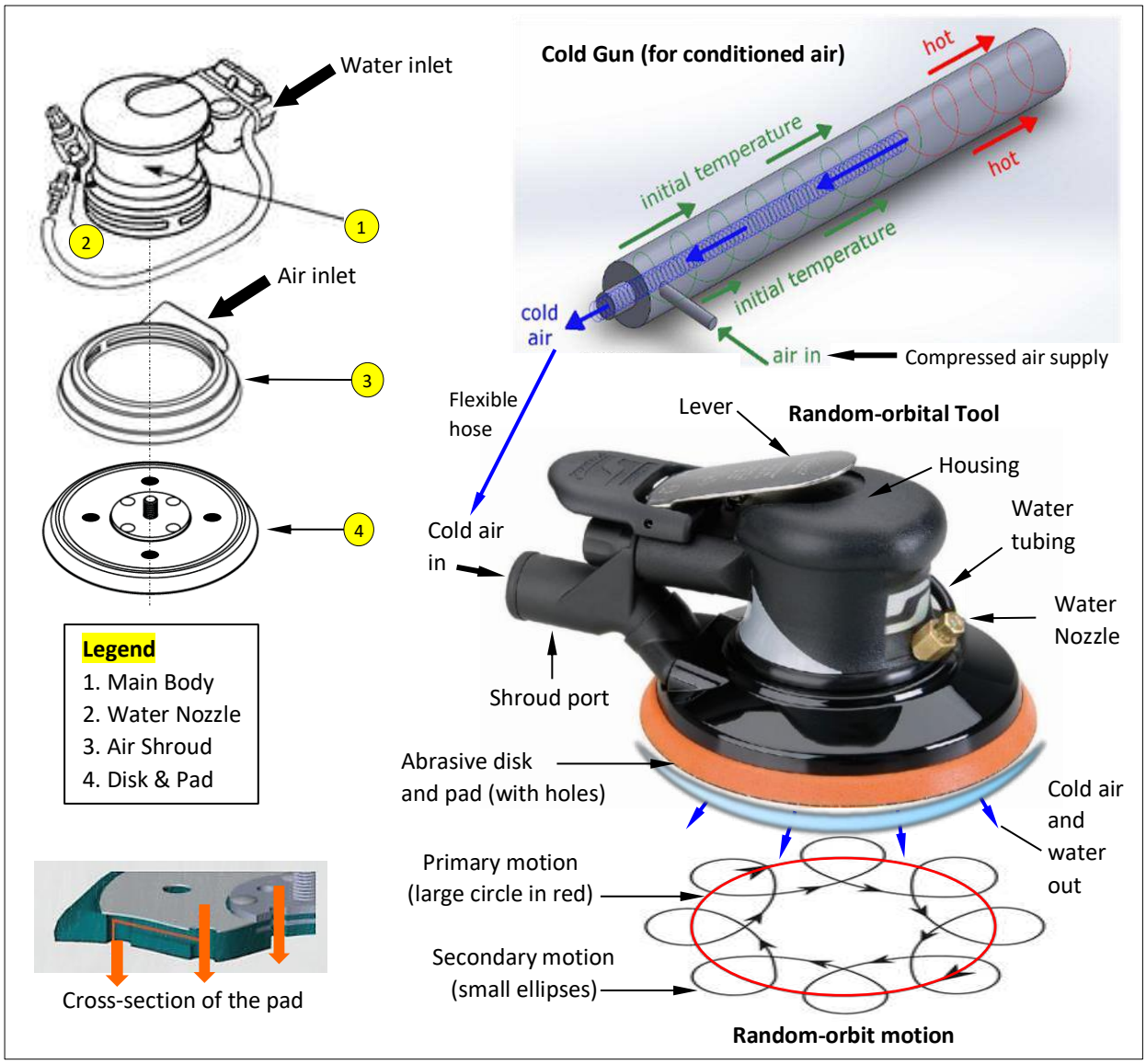

Figure 2. Schematic diagram of the main assembly components for the modified random-orbital tool showing the principle operation of the cold gun and the random-orbit motion of the tool path.

2.2 Abrasive media type

Aluminum oxide (Al_2O_3) and silicon carbide (SiC) are common types of abrasives used for polishing. Because the composition of aluminum oxide is more compatible to the workpiece material (aluminum alloy), silicon carbide is not considered for the experimental trials. Aluminum oxide has a very hard crystal structure with a Mohs value of 9. This strength enables the abrasive to be slowly dulled and hard to fracture, making it suitable for polishing. The grit classification has been established by the association of European abrasive manufacturers (FEPA) where P is the international standard of the FEPA. The workpiece material is made from aluminum alloy 7255-T7751 and the hardness is 170 HV.

The coated abrasive disks are supplied by VSM abrasives (KK712J), and each disk used for the random orbital tool measured 127 mm in diameter. A total of five grit sizes ranging from coarse to fine for P120,

157 P180, P240, P320 and P400 are selected for all the four experimental conditions. The grain size of the
158 abrasive grits is shown in table 1.

159 Table 1. Grit number and corresponding grain size according to FEPA (Europe)

Grit Number	**Grain Size (µm)**
P120	127
P180	78
P240	58.5
P320	46.2
P400	35

160

161 For the single-axis rotary polishing (typical method) using the Toku angle tool, the abrasive disk was
162 down-sized to 100 mm in diameter to match the backing wheel. Figure 3(a) shows the random-orbital
163 tool with the 127 mm disk. Modifications are made to produce 6 large holes (9.4 mm in diameter) and
164 27 small holes (5.0 mm in diameter). The design configuration of the hole pattern was to align with the
165 backing pad holes when attached by the Velcro backing surfaces. This would allow the cooling medium
166 to make direct contact on the treated surface at the heat affect zone. A special feature of the selected
167 abrasive was the unique coating bond over an agglomerated grain structure. This was intended to
168 facilitate slurry formulation under wet conditions where the smaller grains would easily breakdown into
169 finer particles and mix with the deionized water. Figure 3(b) shows the typical grain size ranging
170 between 45 to 48 µm and figure 3(c) shows the typical height of 713.9 µm and width of 945 µm for the
171 agglomerated grain structure.

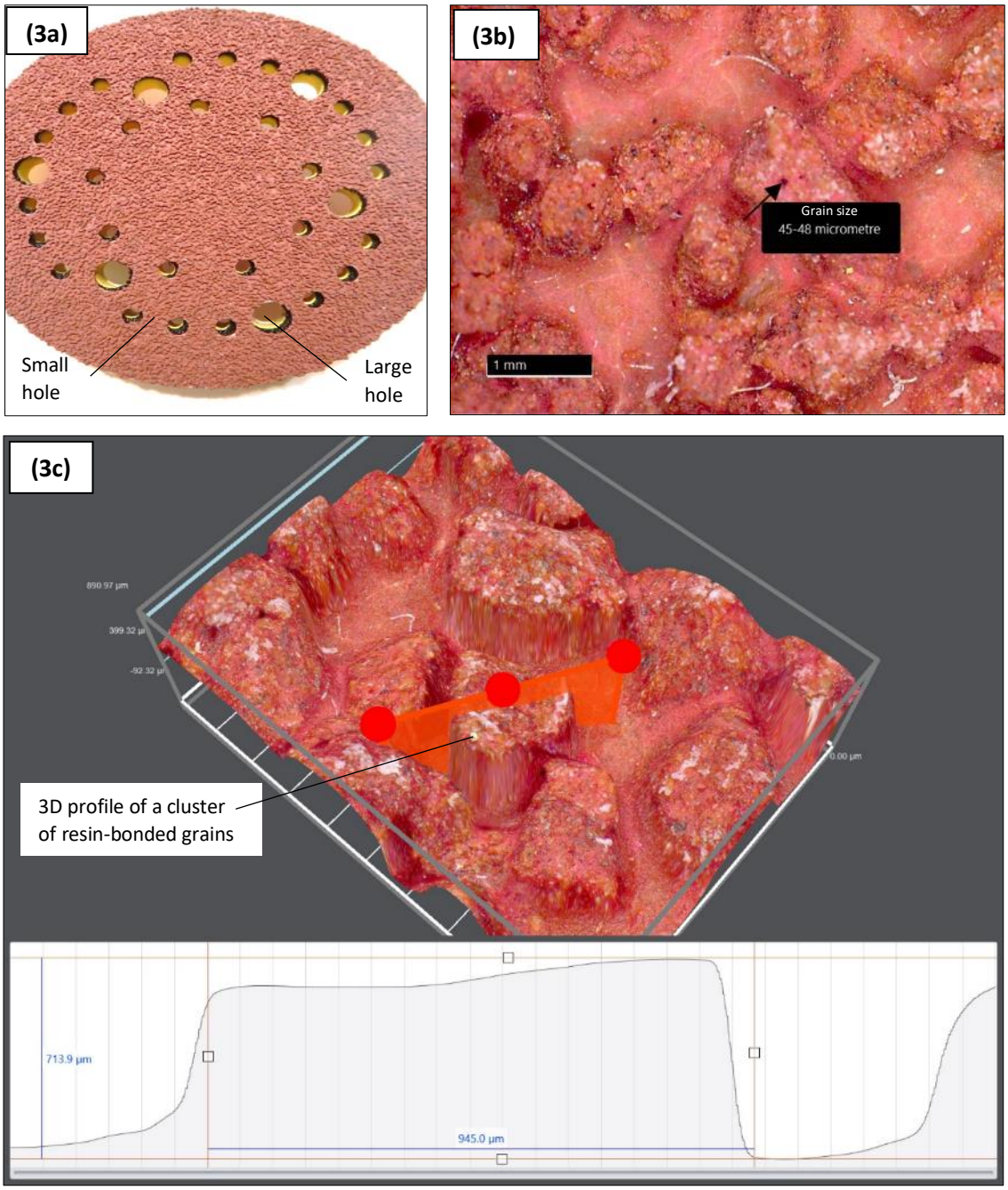

Figure 3. (a) Random-orbital tool with the customized hole pattern in the bonded abrasive disk and backing foam pad to form a matched set, (b) 2D section of an agglomerated abrasive structure of P320 grit. A grain size of P320 grit varied between 45 µm to 48 µm and (c) 3D cross-section of a P320 grit size aggregate showing typical dimensions of 713.9 µm in height and 945 µm in width.

The four conditions assigned for the polishing trials are; condition 1 (dry, ambient air); condition 2 (wet, ambient air); condition 3 (dry, cold air) and condition 4 (wet, cold air). Control parameters for all four conditions are shown in Table 2.

182 Table 2. Table of random-orbital control parameters for the experimental conditions

183

Condition	1 Dry	2 Wet	3 Dry, Cold Air	4 Wet, Cold Air
Fixed parameters				
Process time	9 mins for each grit	9 mins for each grit	9 mins for each grit	9 mins for each grit
Abrasive type	Al_2O_3	Al_2O_3	Al_2O_3	Al_2O_3
Abrasive grit	P120|P180|P240|P320|P400	P120|P180|P240|P320|P400	P120|P180|P240|P320|P400	P120|P180|P240|P320|P400
Abrasive disk diameter	127 mm	127 mm	127 mm	127 mm
No. of large holes	6	6	6	6
No. of small holes	27	27	27	27
Large hole diameter	9.4 mm	9.4 mm	9.4 mm	9.4 mm
Small hole diameter	5.0 mm	5.0 mm	5.0 mm	5.0 mm
Regulated air pressure	620 kPa	620 kPa	620 kPa	620 kPa
Tool speed (max. RPM)	10,000 rpm	10,000 rpm	10,000 rpm	10,000 rpm
Cold air in-line pressure	-	-	300 kPa	300 kPa
Cold air outlet pressure	-	-	172 kPa	172 kPa
Cold air temperature	-	-	15.5 - 16.0°C	15.5 - 16.0°C
Water type	-	Deionised	-	Deionised
Water pH	-	7.41	-	7.41
Water conductivity	-	12.0 - 28.0 µS/cm	-	12.0 - 28.0 µS/cm
Water temperature	-	18°C	-	18°C
Water spray flow rate	-	1.07 L/min	-	1.07 L/min

2.3 Specimens preparation

Five fan blade specimens are used in the polishing trials. The parts are made from forged aluminum alloy 7255-T7751 (AMS 4463), and its material composition shown in Table 3. CNC milling operation is used to produce the as-machined surface condition for the random-orbital and rotary polishing trials.

Table 3. 7255-T7751 Aluminum Alloy Maximum Composition Limits (% weight)

Specimen	**Alloying Elements**									
7255-T7751 Alloy Material	**Zn**	**Cu**	**Mg**	**Zr**	**Mn**	**Cr**	**Ti**	**Si**	**Fe**	**Al**
	8.4	2.6	2.3	0.15	0.05	0.04	0.06	0.06	0.09	remainder
	Others: 0.05									

The leading-edge sections of fan blade specimens are targeted for the random-orbital polishing trials under 4 conditions as shown in figure 4. For the polishing method with the single-axis rotary tool, a fifth fan blade specimen (not shown in figure 4) is used. The fifth specimen belonged to the same batch of machined blades which produced similar scallop height defects. Two additional fan blade specimens processed after shot peen and vibratory finishing (not part of this study) are used for benchmarking to compare the polished surfaces with the semi-final and final condition.

Before the trials are performed, all specimens are loaded in a spray washer machine and treated with alkali solution at 55 °C, and then rinsed with deionized water at ambient temperature. The alkali solution comprised of Ardrox® 6333A (manufactured by Chemetall Asia) mixed with deionized water according to manufacturing specifications. After the washing cycle, the specimens are oven dried at 70 °C and manually wiped by a lint-free cloth to produce a clean and dry surface. Then, each specimen is mounted onto a fixture inside a downdraft polishing booth, where respective sections at the leading edge are measured by a flexible ruler and marked out with a permanent ink pen.

The operator proceeds to use the random-orbital tool with the appropriate abrasive grit for each target section. Polishing time is fixed at 9 minutes for all conditions. After completing the polishing of two samples in each section of the fan blade specimen are marked and cut out by a diamond abrasive wheel Each rectangular sample plate measured approximately 50 mm (length) x 30 mm (width) and is wiped clean by isopropyl alcohol before surface examination.

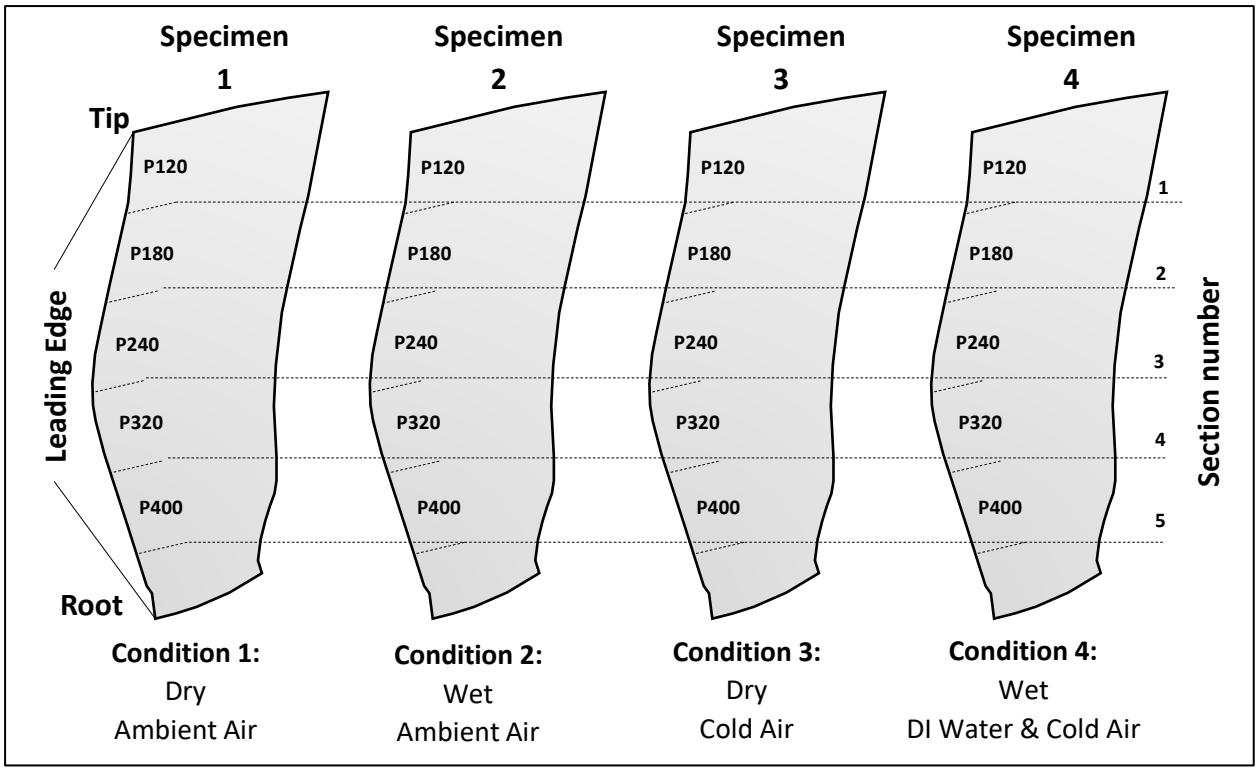

Figure 4. Experimental conditions of 4 aluminum alloy fan blade specimens (7255-T7751) with 5 different grit sizes. The target areas to be finished are at the leading-edge sections, from tip to root demarcated by the section numbers from the dotted lines (Grit sizes P120, P180, P240, P320 and P400).

2.4 Experimental procedure

In the polishing trials for all conditions, the following sequence is executed. The tool is supported by hand to ensure that the abrasive disk remained in contact with the surface during the polishing process. The random-orbital tool is set at a fixed speed of 10,000 rpm by an adjustable knob, and the disk was kept in motion by depressing the lever with the index finger. In figure 5(a), all specimen sections are polished in stationary condition with 50% of the abrasive disk diameter (126 cm^2) making contact to the surface and the remaining 50% over-hang. This is to prevent abrasive encroachment into the adjacent sections.

General polishing sequence for all conditions, 1 to 4: P120 grit for section 1, P180 grit for section 2, P240 grit for section 3, P320 grit for section 4 and P400 grit for section 5. For wet conditions 2 and 4, deionized water with average pH of 7.5 at 18 °C is triggered by the valve at every 3-minute interval. For cold air conditions 3 and 4, the cold gun is started-up for 3 minutes until the air temperature dropped to an average between 15.5 to 16.0 °C (exit temperature of the abrasive disk holes). In figure 5(b), the cold gun is continuously activated by a foot pedal switch throughout the process cycle time of 9 minutes per section at an outlet pressure of around 172 kPa. The 9-minute process time is a standard cycle time that was pre-established for polishing using the existing method.

Figures 5(c) and 5(d) shows the load limit assessment of the tool. Hand pressure is applied in running mode and measured on a scale to simulate a real polishing scenario. Above a load of 4.8 kgf, the tool will stop rotating due to the design limit of the internal motor shaft balancer and bearing. Since the operation is a manual process, the polishing load of around 3.485 +/- 0.1 kgf is measured on the scale beforehand and used as an estimation for all the trials to be conducted. Maintaining the consistency of the load applied is dependent on operator skill in handling and controlling the tool by manual means. To activate the polishing tool, the operator has to ensure that the lever is depressed all the way until it fully bottoms (flush) with the tool housing (groove on the housing below the lever). For each fan blade section, the polishing process is performed for a total time of 9 minutes.

In order to reduce operator variation for the trials, all tests and measurements are performed by the same operator. At the end of the 9-minute polishing time, the wear of the abrasive disk and polishing surfaces are examined. The abrasive life was assessed based on two factors: the density of the abrasive grains remaining on the disk; the capability of the tool to remove scallop heights while producing the required roughness in the surface finish.

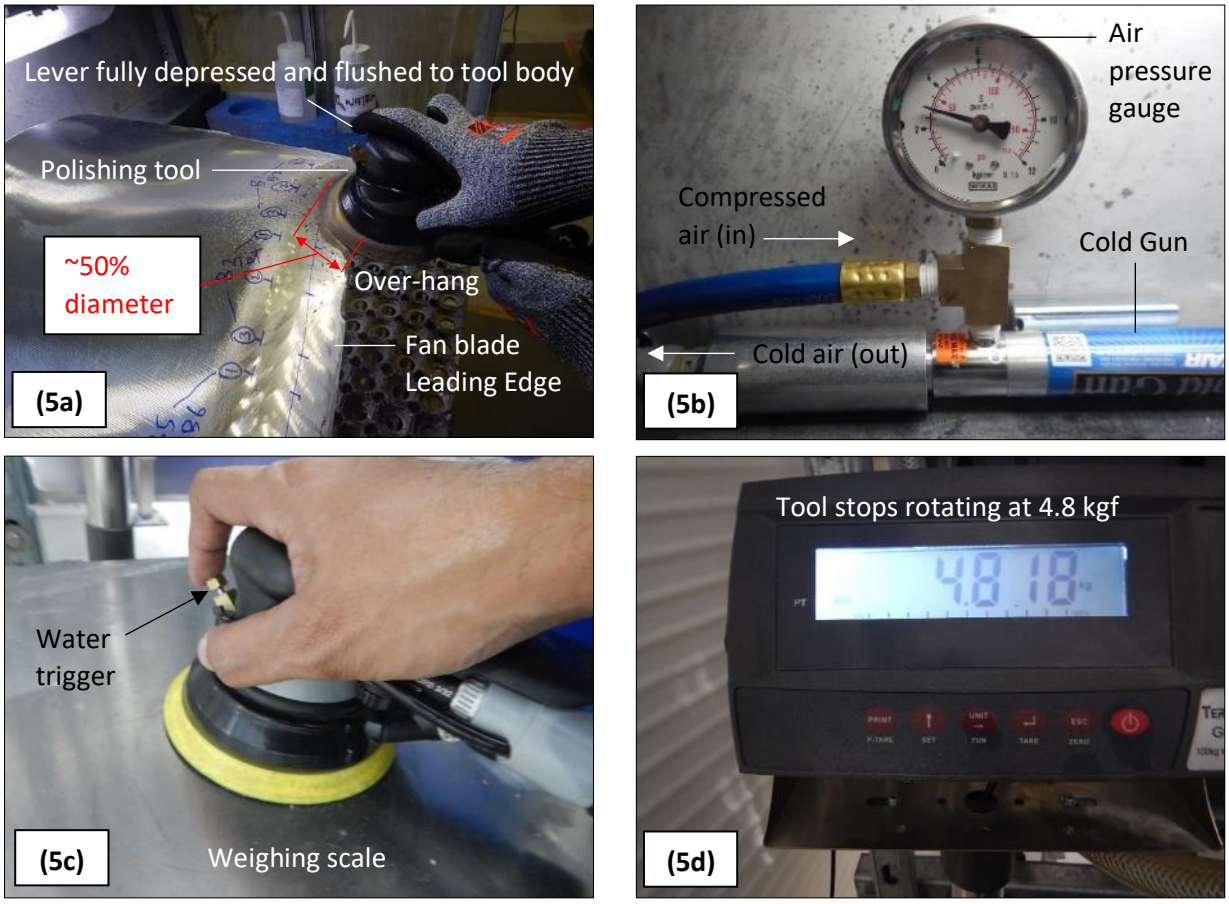

Figure 5. (a) Polishing operation on the specimen, (b) basic components of the cold gun and (c) preliminary testing of the typical load applied on the part and (d) determining the highest load where the tool stops rotating.

2.5 Optical profilometry

The Talysurf CCI 3000 coherence correlation interferometry (CCI) is used for detailed measurement of average height over a surface area (*Sa* parameter) in accordance with ISO25178. The measurement strategy is transverse direction to the forging flow lines which would be the direction that will give the maximum height parameters. The initial surface (as-machined condition) has an average roughness value of *Sa* 1.15 µm. After polishing, the cut-out samples are marked with a cross-hair "+" and placed on a precision X/Y stage for measurement. Because the imaging system is "traversed" through its range by the piezo drive system the focal point is noted for each pixel in the CCD array. Microscopic examination at 20 to 50 x (times) magnification is selected for proper focus and alignment of the cross-hair mark on the sample, as shown in figure 6(a).

For measurement of fine detail, the software configuration is set in XY mode (1024 x 1024 pixels) to give the best greatest lateral resolution. The specimen is mounted flat at normal incidence angle, 90-degree perpendicular to the optical lens in order to capture an accurate pattern. This allows the camera to detect the fringe pattern macro as the scan range needed to fully cover the height of the surface. The stand-off distance between the lens and the specimen is approximately 4.7 mm.

Parameters for auto-stitching mode is optimized to match offset and tilt. The XY scanning area is a 3 x 3 square grid (9 squares, single level) with 20% field-of-view (FOV) and 2.0 µm Z-overlap. The total scanning speed is 217 seconds for one square grid, and the total time taken for one completed measurement is approximately 33 minutes. The 9 squares are stitched together to form a total area of 6.45 x 6.45 mm (41.60 mm^2) for the areal measurement, as shown in figure 6(b).

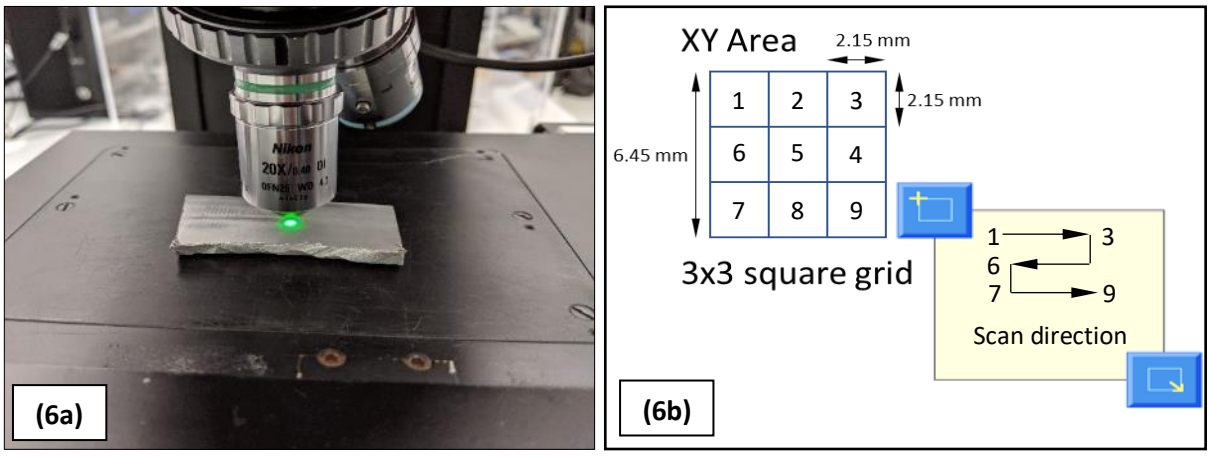

Figure 6. (a) CCI measurement on sample, and (b) X-Y scanning area and direction.

3. Results and discussion

3.1 Surface topography

The Zeiss Smart Zoom 5 digital microscope is used to examine and compare the effects of the experimental conditions on the top surface. The main purpose is to examine the surface texture of different contrasts to uncover defects such as tool lines or scratch marks. The switchable ring-light on the microscope enabled viewing of these deviations by using intensity variations. The surface images of the specimens are shown in figure 7.

In figure 6a, all as-machined specimens have scallop heights on the surface in sections perpendicular to the tool feed direction. This is mainly due to poor machining process. After polishing with P320 grit size, the surfaces show a clear difference between wet and dry condition. Overall, there are three distinct groups of surface textures which is classified for easy identification: group 1- matte with anisotropic finish resulting on single-axis rotary polished sample shown in figure 7(b), group 2 - shiny with fine scratch marks in cross-hatched circular pattern shown in figures 7(c) and 7(e), group 3 - satin with isotropic non-directional finish and homogeneous, resulting on wet orbital polished samples depicted in figures 7(d) and 7(f). All methods under all conditions can remove the sharp-peaked scallop heights.

The single-axis rotary and random-orbital tool are successful in scallop height removal. For dry conditions shown on figure 7(c) and 7(e), the fine scratch marks appear to be shallow and not critical to the surface structure. This will be analyzed and discussed further in sections 3.1 and 3.2.

(7a) Initial as-machined condition with scallop height defect

(7b) Existing method, single-axis rotary tool: Wet, P320

(7c) Random-orbital, Condition 1: Dry, P320

(7d) Random-orbital, Condition 2: Wet, P320

(7e) Random-orbital, Condition 3: Cold Air, P320

(7f) Random-orbital, Condition 4: Wet, Cold Air, P320

Figure 7. Images before and after polishing for 9 minutes with P320 grit size: (a) Initial, as-machined condition with scallop height defect, (b) Existing polishing method with single-axis rotary tool, wet condition, (c) Random-orbital method, condition 1; dry, (d) Random-orbital method, condition 2; wet, (e) Random-orbital method, condition 3; cold air, (f) Random-orbital method, condition 4; wet, cold air.

The typical surface finish for the fan blade is *Ra* 2.0 µm (maximum threshold limit). However, a nominal range of *Ra* from 0.8 to 1.0 µm is an ideal target for post-polishing, as the surface undergoes gradual increment in roughness to final condition at vibratory finishing.

The surface topography results of the polished samples are presented in Table 5. An average of 3 horizontal line readings are scanned for each sample and measured at the worst condition as observed visually. Overall, it can be observed that surfaces polished by the random-orbital method produced lower *Ra* values as compared with the single-axis rotary method. All the values are within the maximum limit of $Ra \leq 2.0$.

The peak-to-valley heights (*Rz*) for the random-orbital method are all lower than the single-axis rotary method, except for wet condition without cold air. The random-orbital method under wet and cold condition has a higher *Rz* but lower *Ra* as compared to the as-machined surface. Dry condition for random-orbital method has the lowest *Ra* value, while dry, cold air alone has the lowest *Rz* value.

Table 5. Results of P320 results showing amplitude roughness parameters – *Ra* and *Rz*

Polishing method	N/A	Rotary, single-axis	Random-Orbital	Random-Orbital	Random-Orbital	Random-Orbital
Condition	As-machined	Wet	Dry	Wet	Dry, Cold Air	Wet, Cold Air
Process time	N/A	9 mins	9 mins	9 mins	9 mins	9 mins
Abrasive grit	N/A	P320	P320	P320	P320	P320
Roughness parameters (µm)						
Ra	0.9	1.227	0.318	0.969	0.338	0.821
Rz	4.3	6.667	3.951	6.925	3.827	5.864

The visual results observed in figure 6 give an indication that random-orbital method under wet conditions produces a smoother finish than dry conditions. However, this may be in contradiction to the with the results in table 5. In figures 8(a) to 8(d), the images may clarify this ambiguity. Although the surfaces in figure 8(a) and 8(c) have lower *Ra* values, there is evidence of fine tool marks. Figures 8(b) and 8(d) indicate that upon detailed analysis, the surface textures appear to be coarse instead of smooth.

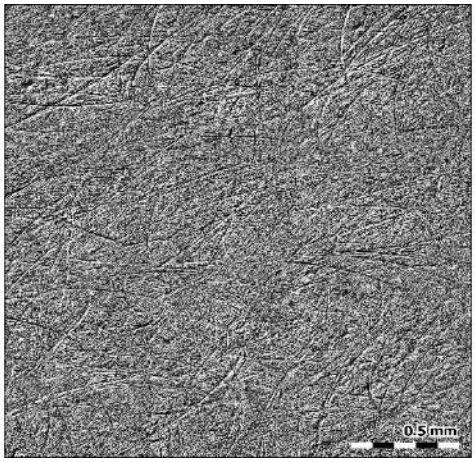

(8a) Random-orbital, Condition 1: Dry, P320 grit

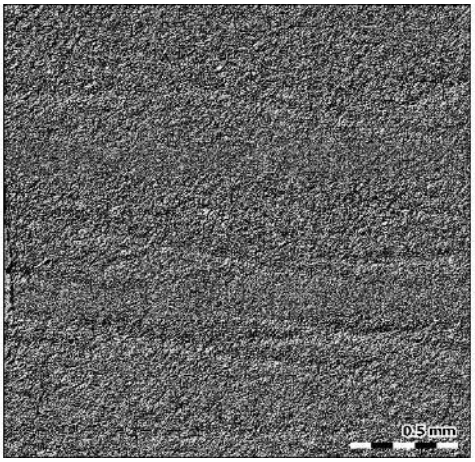

(8b) Random-orbital, Condition 2: Wet, P320 grit

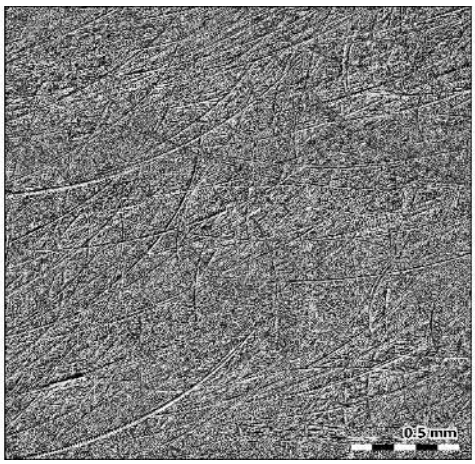

(8c) Random-orbital, Condition 3: Cold Air, P320 grit

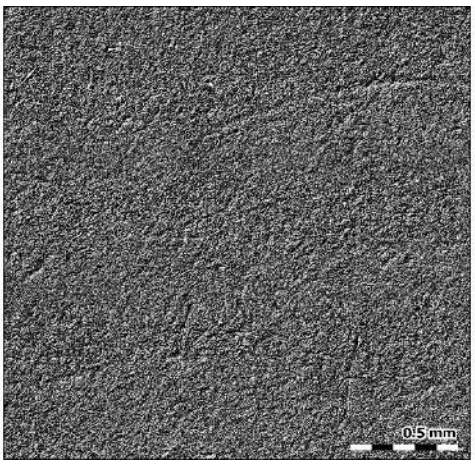

(8d) Random-orbital, Condition 4: Wet, Cold Air, P320 grit

Figure 8. 2D surface topography comparison after random-orbital polishing for 9 minutes with P320 grit size: (a) Condition 1; dry, (b) Condition 2; wet, (c) Condition 3; cold air, (d) Condition 4; wet, cold air. Measurement instrument used was Talysurf CCI 3000.

To rule out variation by using data from the P320 grit alone, the results of the full experimental trials with other different grit sizes are shown in figures 9 and 10. The trend for other grit size comparison prove that indeed conditions 2 and 4 have a higher *Ra* and *Rz* than conditions 1 and 3. Overall, all the specific grit sizes for conditions 1 and 3 produce an *Ra* of below 0.8 µm. Having parts polished to generate low *Ra* and *Rz* values area considered partially completed, as the parts would eventually be processed to reach higher *Ra* and *Rz* values.

Generally, a minimum *Rz* of 5 µm and a typical *Ra* value of approximately 1 µm are manufacturing-known values in the final process at vibratory finishing. Conditions 2 and 4 (P320 grit size) have met the *Ra* and *Rz* values close to the final process. The trend of producing both low *Ra* and *Rz* values for condition 1 across all grit sizes is similar to condition 3. Additionally, it can be noted that the coarser

grains of P120 grit size does not generate significantly rougher surfaces for condition 1 and 3, as compared to conditions 2 and 4.

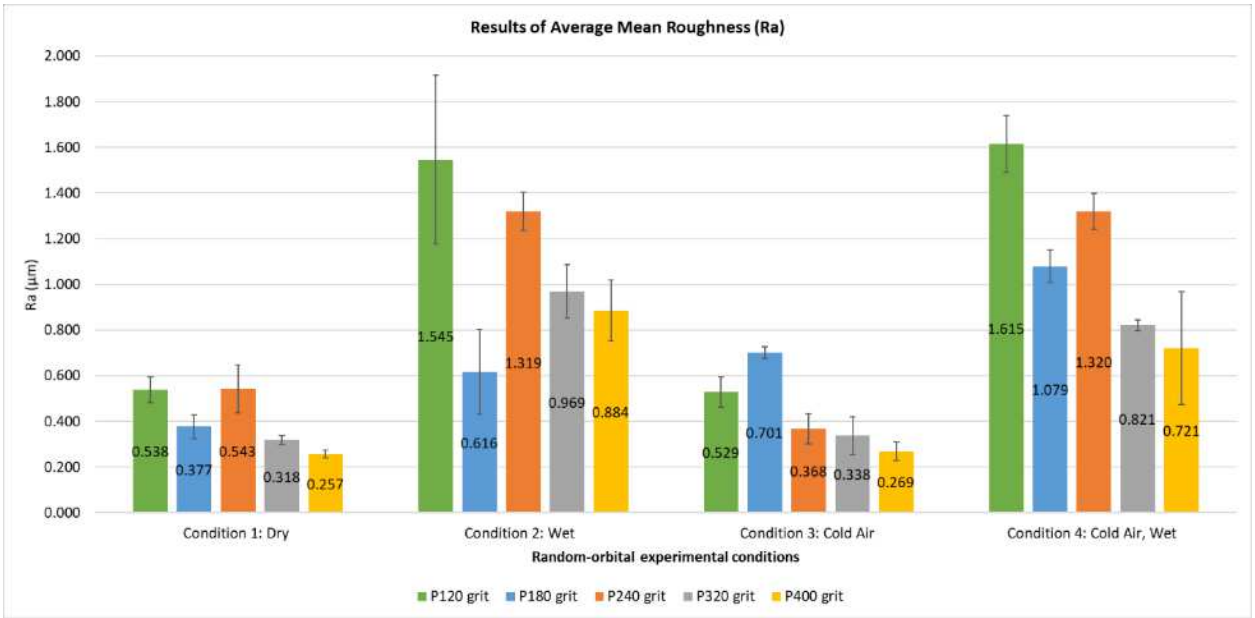

Figure 9. Results of *Ra* for all conditions with P120, P180, P240, P320 and P400 abrasive grit sizes. (Measurement instrument used was Talysurf CCI 3000).

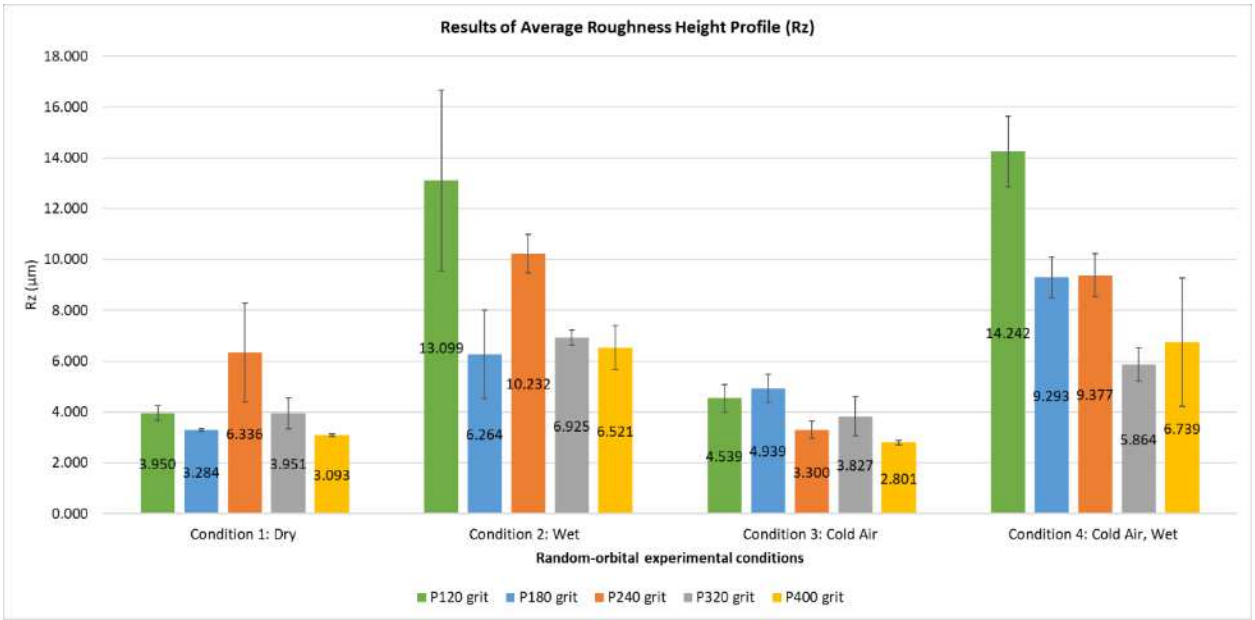

Figure 10. Results of maximum height profile (*Rz* parameter) for all conditions with P120, P180, P240, P320 and P400 abrasive grit sizes. Measurement instrument used was Talysurf CCI 3000.

The isometric image is shown in figure 11 illustrating the different pre- and post-polishing topographies with P320 grit size abrasive. Figure 11(a) shows as-machined scallop heights as a result of poor machining. The peak features are sharp and pointy. Existing polishing method in figure 11(b), show that the material removed is high (indicated by the blue spectrum), with evidence of grooving indicated by the darker blue lines. This is due to the abrasive grain ploughing the ductile specimen and the

341 thickness of the leading edge may be undersized as a result. In the process, a foreign particle (inclusion)
342 is found embedded into the surface (see Fig 11(b)).

343 The ploughing phenomenon is a common occurrence for single-axis rotary tools at high cutting speeds
344 where the abrasive interacts with the specimen, leaving small particles embedded in the top surface
345 structure. For specimens polished in dry conditions shown in figures 11(c) and 11(e), there is no
346 noticeable variation at first glance. The application of deionized water is seen to be the key contributing
347 factor that greatly influence the surface texture of the specimens as shown in figures 11(d) and 11(f).

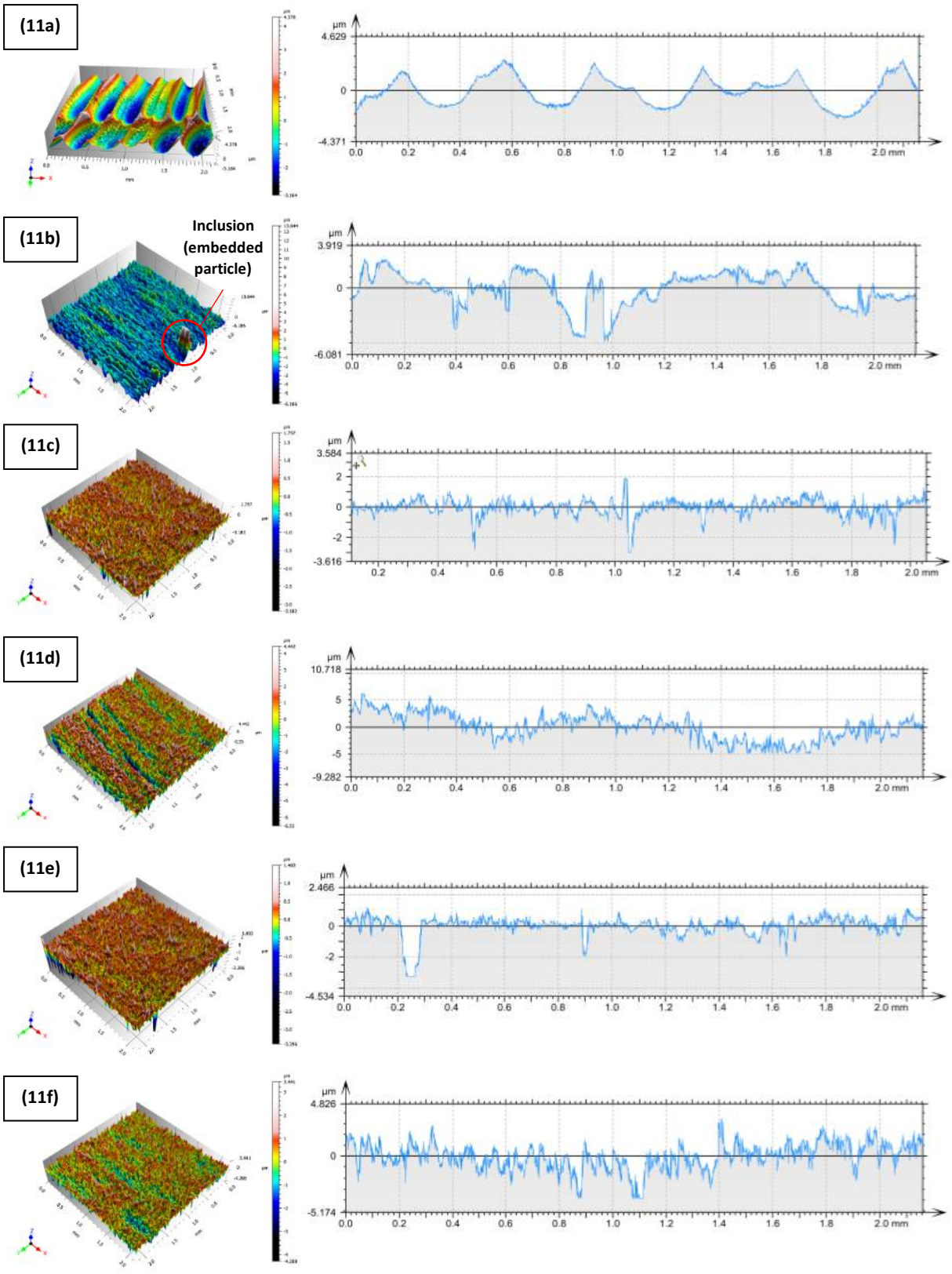

Figure 11. Surface profiles showing peak and valley by coherence correlation interferometry (CCI): (a) Initial, as-machined condition with scallop height defect, (b) Single rotary axis, wet, P320, (c) Random-orbital method, condition 1; dry, P320 (d) Random-orbital method, condition 2; wet, P320 (e) Random-orbital method, condition 3; cold air, P320, (f) Random-orbital method, condition 4; wet, cold air, P320. Measurement instrument used was Talysurf CCI 3000.

Table 6 shows the results of post-polished areal surface roughness (*Sa and Sz*) with P320 grit size. Overall, the trend for all groups is similar to the amplitude roughness data in table 5. However, the difference is the areal peak-to-valley heights (*Sz*) for the random-orbital method are all lower than the single-axis rotary method, including for wet condition without cold air. The other difference is that dry condition with cold air for random-orbital method produces the lowest *Sa* and *Sz* value, indicating that the lack of texturing effect for the subsequent coating application to be effective.

Table 6. Results of P320 grit size showing areal roughness parameters – *Sa*, and *Sz*

Description	As-Machined	Rotary, single-axis	Random-Orbital	Random-Orbital	Random-Orbital	Random-Orbital
Condition	Initial	Wet	Dry	Wet	Dry, Cold Air	Wet, Cold Air
Process time	N/A	9 mins	9 mins	9 mins	9 mins	9 mins
Abrasive grit	N/A	P320	P320	P320	P320	P320
Roughness parameters (µm)						
Sa	1.15	1.39	0.35	1.25	0.29	0.78
Sz	7.54	19.83	4.94	10.97	4.88	7.73

Figure 12 compares the *Sz* parameter of P320 grit size for the polishing conditions. Conditions 1 and 3 show potential in producing similar profiles, both values significantly lower than the initial condition and existing method. Conditions 2 and 4 have a higher *Sz* value than 1 and 3, but both lower than the single-axis rotary tool. Overall, condition 4 is leaning towards the eventual *Sz* value (9 µm) when the actual part reaches its final finishing process using vibratory finishing. This means that the surface could benefit from less treatment work to be processed prior to the final stage.

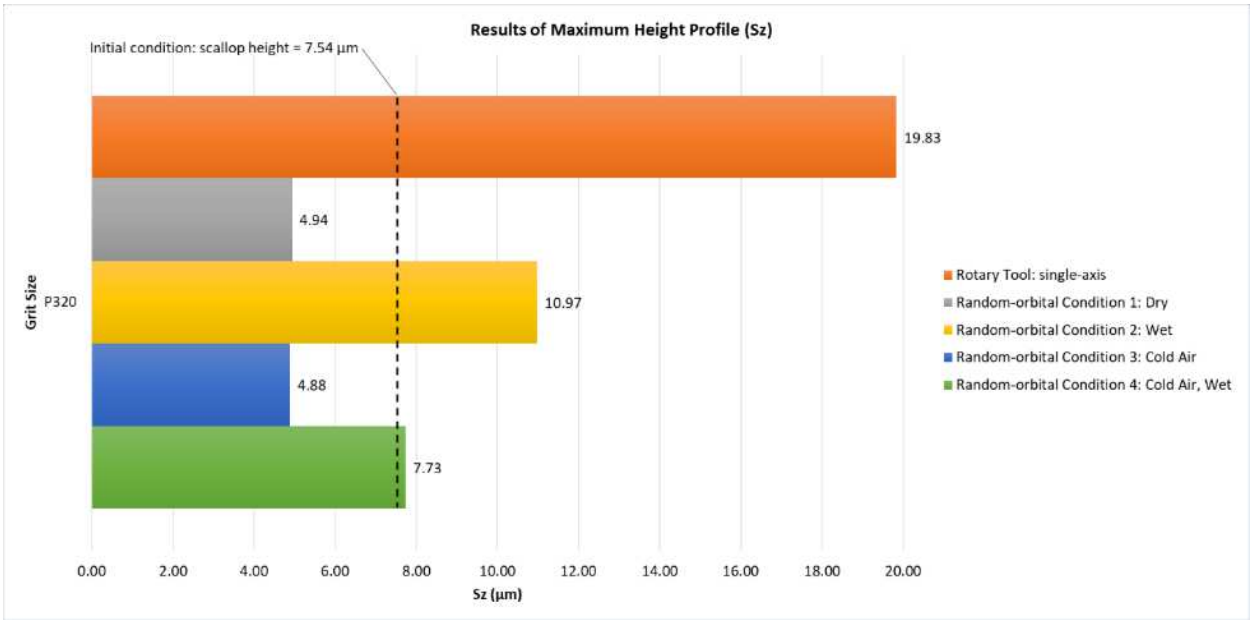

Figure 12. Results of maximum height profile (*Sz* parameter) for all conditions with P320 abrasive grit sizes. Measurement instrument used was Talysurf CCI 3000.

In figure 13, the results of *Sa* parameter for all grit sizes will indicate any variances or anomalies when the abrasive particle size is changed. Firstly, it can be noted that all the grit sizes for conditions 1 and 3 are able to produce a lower roughness as compared to initial surface condition. An outlier is noted for P180 grit size for condition 3, where the trend differs from the other conditions (higher *Sa* than P120 and P240 grit size).

Specific to P320 grit size, only condition 2 produces a *Sa* value is marginally higher than initial condition after polishing (Δ0.096 µm). In order to produce a *Sa* lower than the initial condition, it is necessary for condition 2 to use a finer grit size of P400. Another observation is found in condition 3, where there is no significant drop in *Sa* value between P320 and P400 grit size. The data suggests that the abrasive reaches its saturation point and is unable to lower the *Sa* value any further.

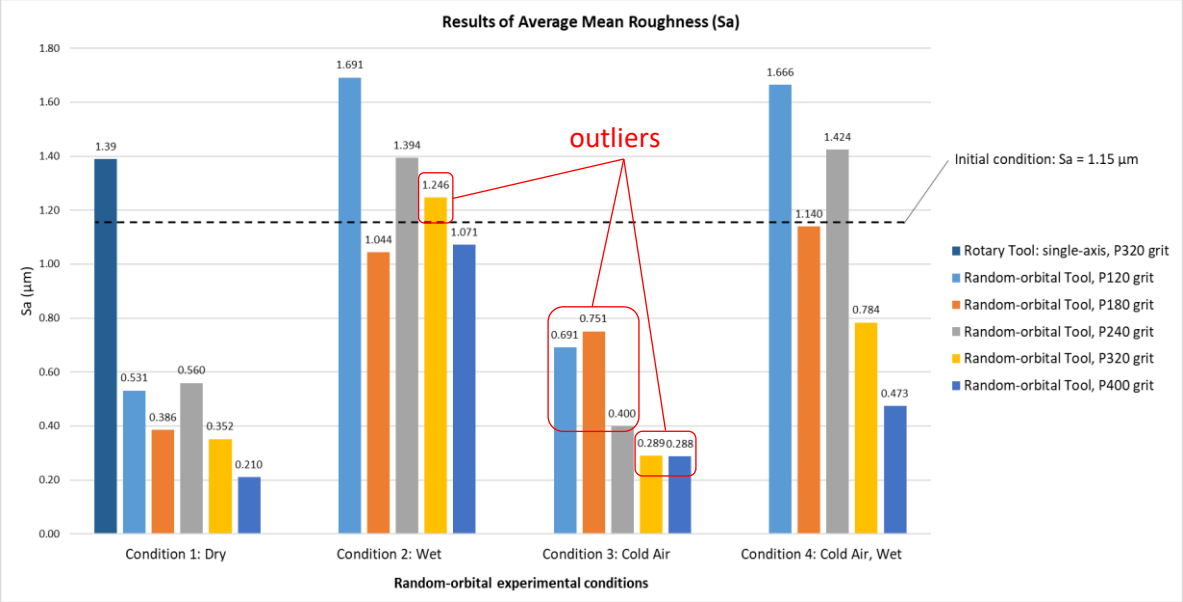

Figure 13. Results of average mean roughness (*Sa* parameter) for all conditions with P120, P180, P240, P320 and P400 abrasive grit sizes. Measurement instrument used was Talysurf CCI 3000.3.2

A furrow is defined as depressions in the surface structure caused by mechanical abrasion. A surface texture with higher furrow depth and density will promote better adhesion to paint or coating layer due to the enhanced anchoring effect in the structure. For the random-orbital motion, the dislodged abrasive particles will start rolling between the surface of the disk and the workpiece. In this material removal mechanism, the grain is forced into the sample material, thus creating a series of furrows.

The results in figure 14 show the maximum depth, mean depth and the mean density of these furrows compared against the various conditions for P320 grit size. As expected, the wet conditions 2 and 4 are noticed to have larger depths as compared to dry conditions 1 and 3. This phenomenon can be understood as furrows not caused by cutting action alone, instead, the distinct tracks are deepened by particles tumbling over the surface due to the meniscus force of the water. It is the free moving abrasives present in the slurry that create swallow valleys in the surface, resembling that of three-body abrasion.

The furrows are enhanced by the meniscus force produced due to the water surrounded by the abrasive [14].

The key observation to note is that all conditions for the random-orbital method produces shallower furrows of lower mean and maximum depth as compared with the single-axis rotary method with P320 grit size. However, only condition 4 produces an increase of 5.52 cm/cm^2 in mean density A higher furrow density would suggest that the surface texture is favorable in promoting higher coating adhesion strength. It is possible to verify the effect of temperature between conditions 2 and 4, in order to understand why condition 4 shows evidence of furrows with less significant depths. The lowered temperatures of condition 4 and the induced air stream may change the viscous flow in the sliding mechanism, evacuating a portion of the abrasive particles, thus reducing the rolling effect.

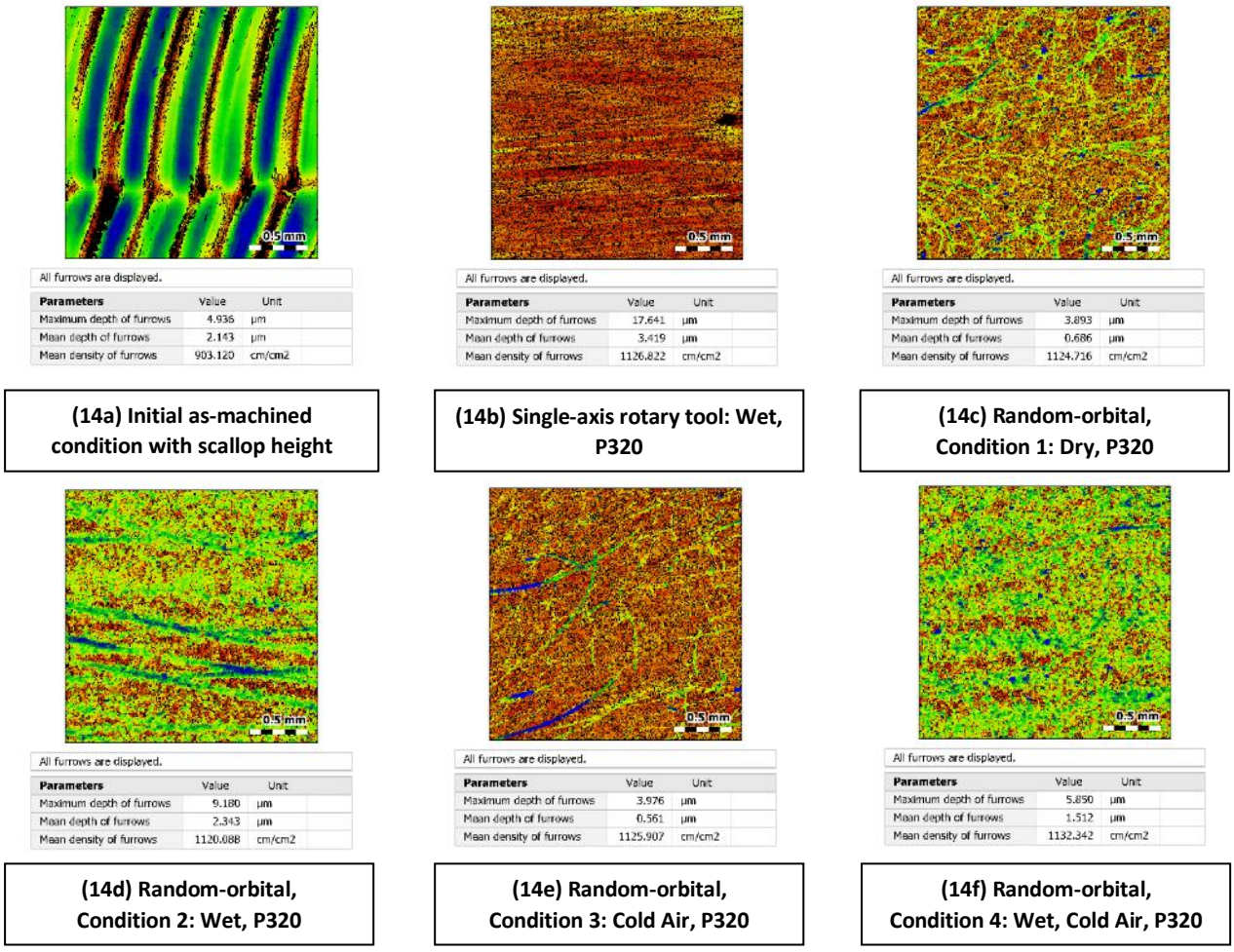

Figure 14. 3D image and parametric report of furrows by coherence correlation interferometry (CCI) after polishing for 9 minutes with P320 grit size: (a) Initial, as-machined condition with inherent step mark defect, (b) Single rotary axis, wet condition, (c) Random-orbital method, condition 1; dry, (d) Random-orbital method, condition 2; wet, (e) Random-orbital method, condition 3; cold air, (f) Random-orbital method, condition 4; wet, cold air.

3.2 Effect of medium on microstructure, hardness and tensile stress

A common way to examine the sub-surface condition of the polished samples is by metallurgical analysis of the cross-section. For this study, all samples polished with P320 grit size are evaluated and discussed. The fan blade specimens are prepared by marking and sectioning the mid-point of each sample in two directions (longitudinal and transverse). A precision cutting wheel is used for this task and operated at 3,000 rpm with a feed-rate of 15.2 mm/min. After this, the samples are processed in a hot mounting machine. The polishing process is done with a grinding machine (Buehler Ecomet 300) and the sample mounts are lapped with diamond suspension. The metallographic procedures for sample preparation are in the following order:

1. Hot-mount with phenolic resin or thermoplastic acrylic
2. Apply a force of 5 N
3. Polish with silicon carbide (SiC) grit papers
4. For each grit type is subjected to a polishing duration 30 sec
5. Lapping compound: 3 µm diamond suspension – 1 minute
6. Rinse
7. 0.05 µm diamond suspension – 1 minute
8. Keller's etchant by swab

The micrographs of the cross-sectioned coupons are shown in figure 15. All samples are examined under 500x magnification with white light and checked for evidence of distortion and defect in the surface structure.

For conditions 1, 2 and 4, there were no visible evidence of any such defects. For condition 3 (lateral direction) shown in figure 15(c), there is a gouge defect measuring approximately 25 µm in length and 5 µm in depth, thus exceeding the criteria of 5.0 µm. In the transverse direction for condition 3, it is noticeable that there is unevenness in the surface profile.

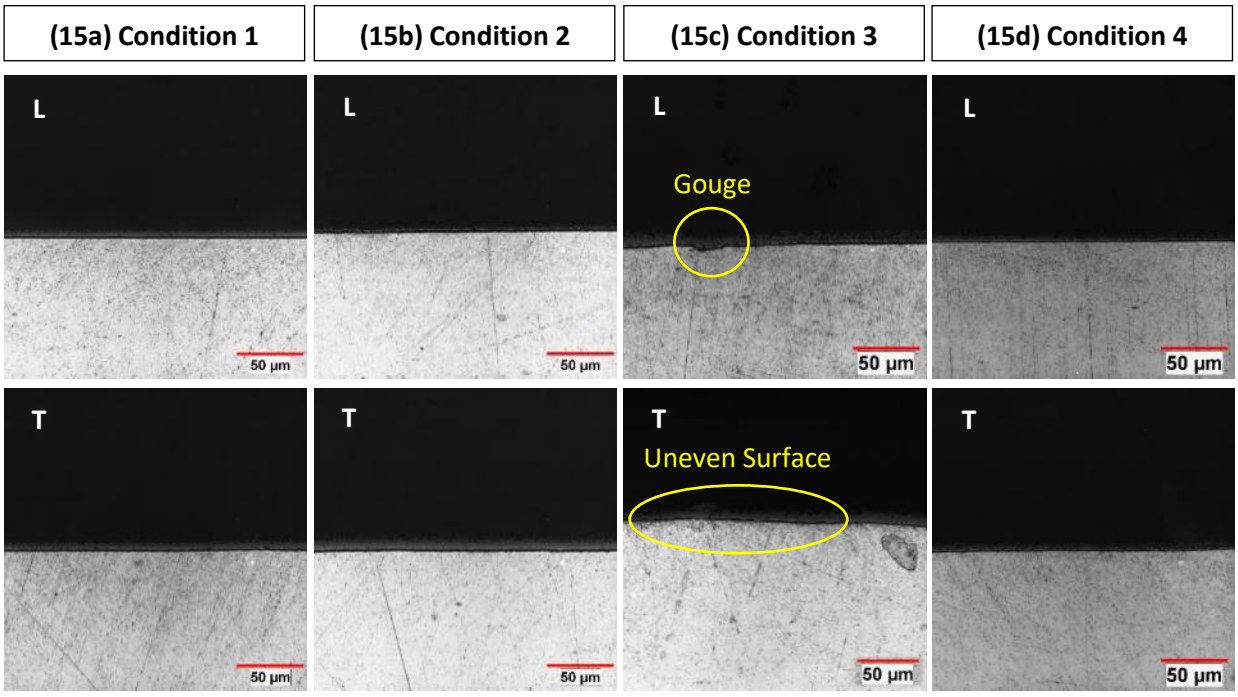

436 Figure 15. (a) to (d) Conditions 1 to 4: Microstructure of the random-orbital polished specimens with
437 P320 grit size – lateral (L) and transverse (T) direction

438 Hardness testing of the polished samples is performed using a Vickers indenter (Falcon 250 Innovatest)
439 with a diamond pyramid tip as shown in figure 16. The hardness tester and procedures are performed
440 according to the standard test methods of ASTM E92-82 and ASTM E384. An average of three hardness
441 indentation readings are taken by applying a load of 300 gF (2.9 N) and a dwell time of 10 seconds at
442 the center region of the specimens.

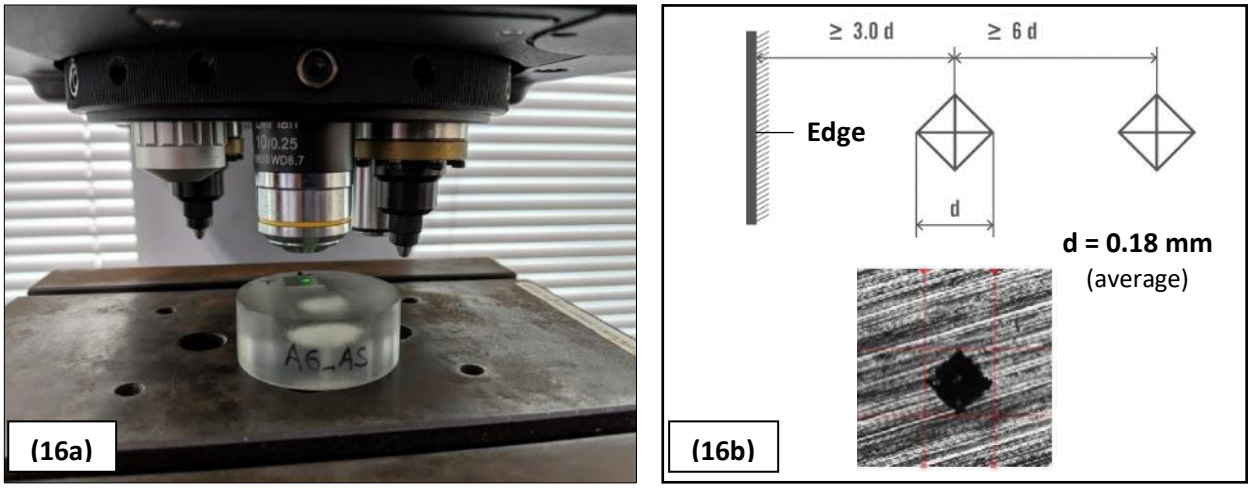

443

444 Figure 16. (a) Vickers hardness tester with sample mount and (b) indentation strategy on the
445 sample surface (average of 3 readings taken)

446 The hardness test results are shown in figure 17. The hardness values of all polished specimens under
447 conditions 1, 3 and 4 are marginally higher than the as-machined condition. The single-axis rotary
448 method has a highest increase in hardness by 12.2 HV, whereas the random-orbital polishing for
449 condition 2 has an opposite effect with a reduction in hardness by 18.23 HV. For the single-axis rotary
450 polishing, the higher hardness can be attributed to the cutting speed of the tool, where the fixed direction
451 generates a higher abrasive action.

452 The increased hardness is attributed to the decrease in grain size and small particles of intermetallic
453 compounds, while processed specimens submerged in water exhibit lower hardness [15]. The water-
454 cooled specimen for condition 2 shows lower hardness than the rest, suggesting that the meniscus force
455 due to the surface tension of water between the abrasive disk and specimen has an effect on the hardness.
456 This effect is minimal for condition 4 because the water layer is disrupted by the continuous stream of
457 cold air on the surface. Therefore, the surface tension for condition 4 is regarded as negligible as it
458 neither creates any defect nor adversely affects the microstructure of the surface.

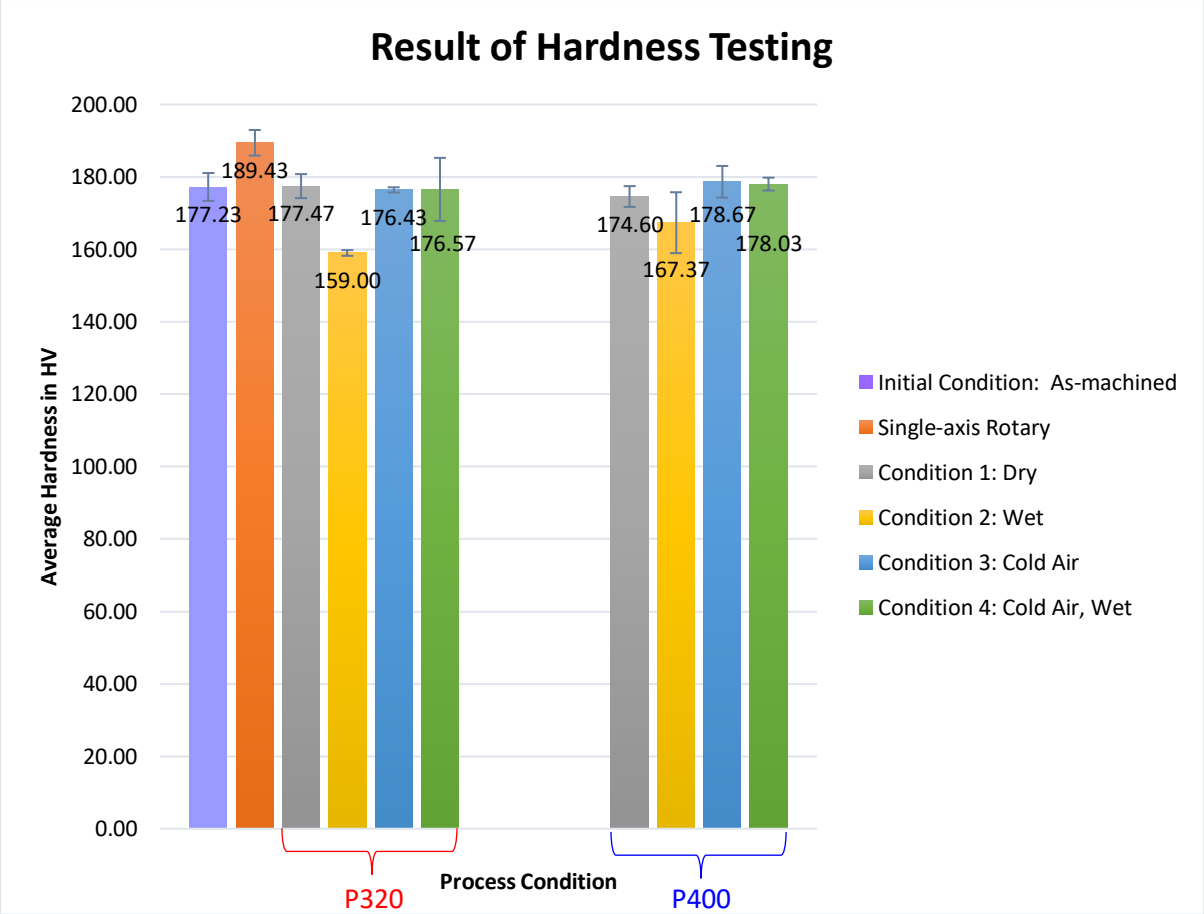

459

460 Figure 17. Micro-hardness test result for P320 grit size polished samples - average of 3 indentations for
461 each condition carried out.

462 According to ISO 6507-1:2005, the Vickers (HV) hardness is calculated using following formula:

463 $$\mathrm{HV} = 0.1891 * \frac{F}{d^2} \ [\mathrm{N/mm^2}] \quad \text{Eq 1}$$

464 where d is the average of the two diagonals of the imprint and F is the applied load.

465 The yield stress (tensile yield) can be approximated from the hardness (given in HV) as follows:

466 $$\sigma_u = \frac{HV}{0.3} \qquad [\mathrm{MPa}] \quad \text{Eq 2}$$

467 Take an example for condition 4 of hardness value 178 HV. Applying the formula in Eq 2, the yield
468 stress σ_u is calculated to be 593 MPa, which correlates to the forging material specification in Table 7.
469 It can be concluded that the overall hardness and strength for conditions 1, 3 and 4 is not significantly
470 changed with random-orbit polishing method.

471 Table 7. Forging material properties for aluminum alloy specimen T7255

Alloy/Temper	**Dir.**	**7255 (forging material)**
Tensile Strength, F_{tu}, ksi (MPa)	L	91 (627)
	LT	91 (627)
Tensile Yield, F_{ty}, ksi (MPa)	L	88 (607)
	LT	86 (593)

Elongation, %, 4D	L	9
	LT	7
Comp. Yield, F_{cy}, ksi (MPa)	L	88 (607)

By factoring the hardness values in Eq 2, the yield stresses are plotted out for full processes in the manufacturing life-cycle. As shown in figure 18, the abrasive process begins with milling (as-machined), followed by polishing, then shot-peening, and finally vibratory finishing.

By focusing on the random-orbit process, condition 1, 3 and 4 perform equivalent to as-machined condition, with the yield stress matching very close to 590 MPa. Comparing the final the manufacturing stage at vibratory finishing, the part will have its yield stress increase to around 650 MPA (Δ60 MPa).

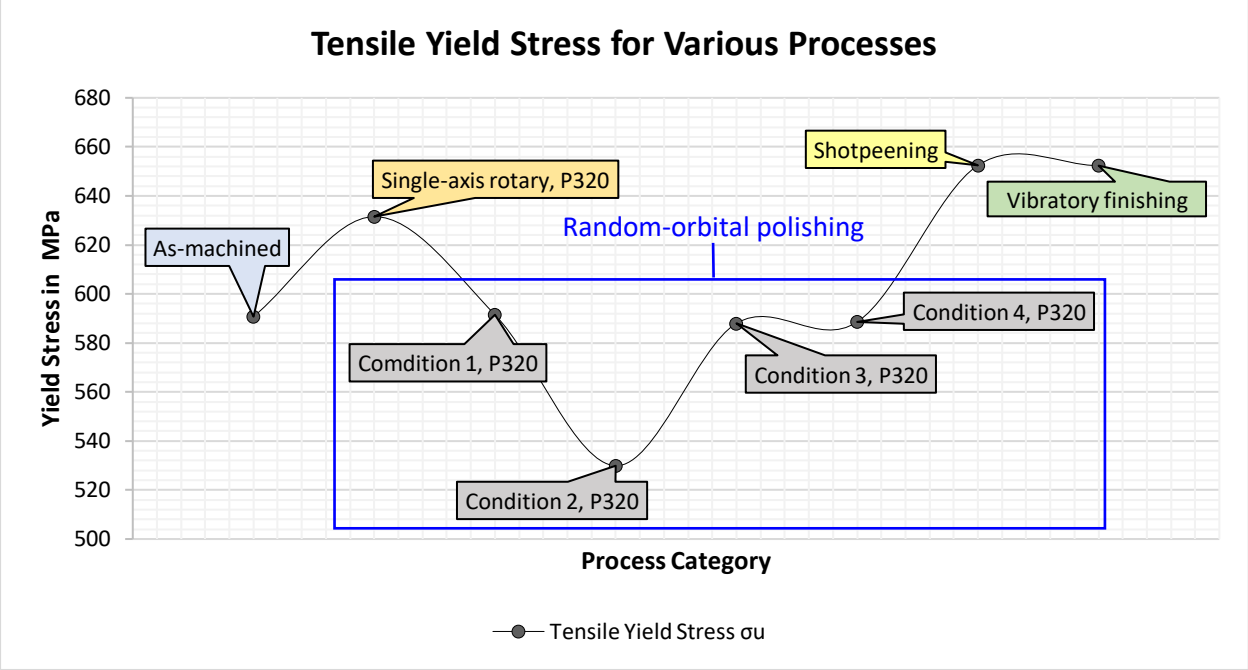

Figure 18. Approximate tensile yield stress calculated based on average hardness values.

3.3 Effect of cold air and water medium on the abrasive disk

At this stage in the evaluation, condition 4 is found to have favourable results where the hardness and microstructure are validated. The other area of study is the abrasive disk life for the various conditions by the random-orbital method. For wet conditions 2 and 4, it is important to determine the proper wettability of the abrasive disk at the fluid state and to regulate the homogeneous dispersion of abrasive particles onto the workpiece surface. Wet application has some drawbacks such as messy operation due to the splatter of the abrasive fluid at the adjacent areas and higher abrasive disk wear.

A high precision Ohaus PX323JP model analytical weighing balance is used to measure the weight loss of the abrasive disk after polishing as shown in figure 19(a). Before measurements, the abrasive disks are cleaned by a pneumatic gun at 15 psi air pressure for approximately 3 minutes and until no visible traces of loose dust or water are present on the abrasive disk surface. Then, a section of each abrasive

disk measuring approximately L10 mm x W10 mm is cut out and inspected by digital microscope using dino-lite edge model AM7915MZTL.

From the images shown in figure 19(b), the fixed abrasive grains on the disk for wet conditions 2 and 4 is observed to have the highest amount of wear. The grit sizes of P120, P182, P240 and P320 for condition 4 is observed to be less worn as compared to condition 2. Perhaps this is due to the minimum quantity lubrication (MQL) technique inherent for condition 4, with the formation of an aerosol mist during tool activation. This is key in understanding that the lack of additional air evacuation for condition 2 would result in flooding of the abrasive disk. It is important to note that a certain amount of wettability is crucial to extending the life of the abrasive disk, as proven in condition 4. The results imply that the wetter the disk, the higher the friction, thus wearing the abrasives at a faster rate. The important lesson from the experimental trials is that the abrasives must be moist and not excessively wet, in order for better abrasive performance.

Dry conditions 1 and 3 display similar trends in abrasive wear pattern throughout the grit size range. Comparing amongst all conditions for P320 grit size only, the data indicates that using water in the process shortens the abrasive disk life significantly. Also, condition 3 is noticed to have a higher degree of particle loading (greyish white colour) as compared with condition 1. This may cause the abrasive to be blunt and lose its effectiveness in the polishing process. The embedment of soft and sticky aluminum oxide particles may cause particle embedment or even damage a portion of the workpiece surface.

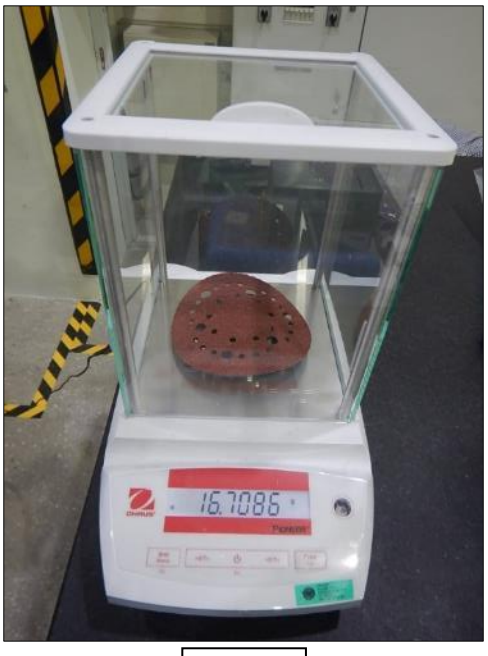

(19a)

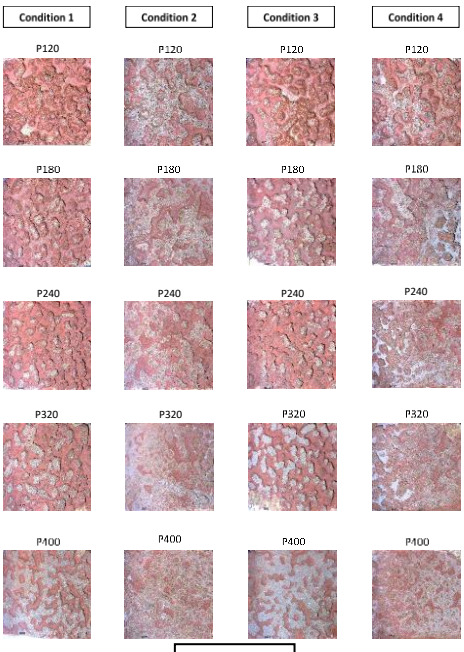

(19b)

Figure 19. (a) Abrasive disk is weighed before and after random-orbital polishing, and (b) abrasive disk samples inspected by digital microscope after 9 minutes of random-orbital polishing.

The intent of this study is not only surrounding the feasibility of the new method, but also to discover whether it has any potential of productivity improvement and cost avoidance. From the abrasive disk life study results shown in figure 20, conditions 2 and 4 experienced the highest weight loss as compared with conditions 1 and 3 after random-orbital polishing. In a real scenario for fan blade production, frequent replacement of abrasive disks will increase wastages and consumable costs. As a rough estimate, the random-orbital polishing for conditions 2 and 4 would require a quantity of five disks to polish a full fan blade leading edge section. Whereas, polishing in conditions 1 and 3 requires only one disk for the same polishing work.

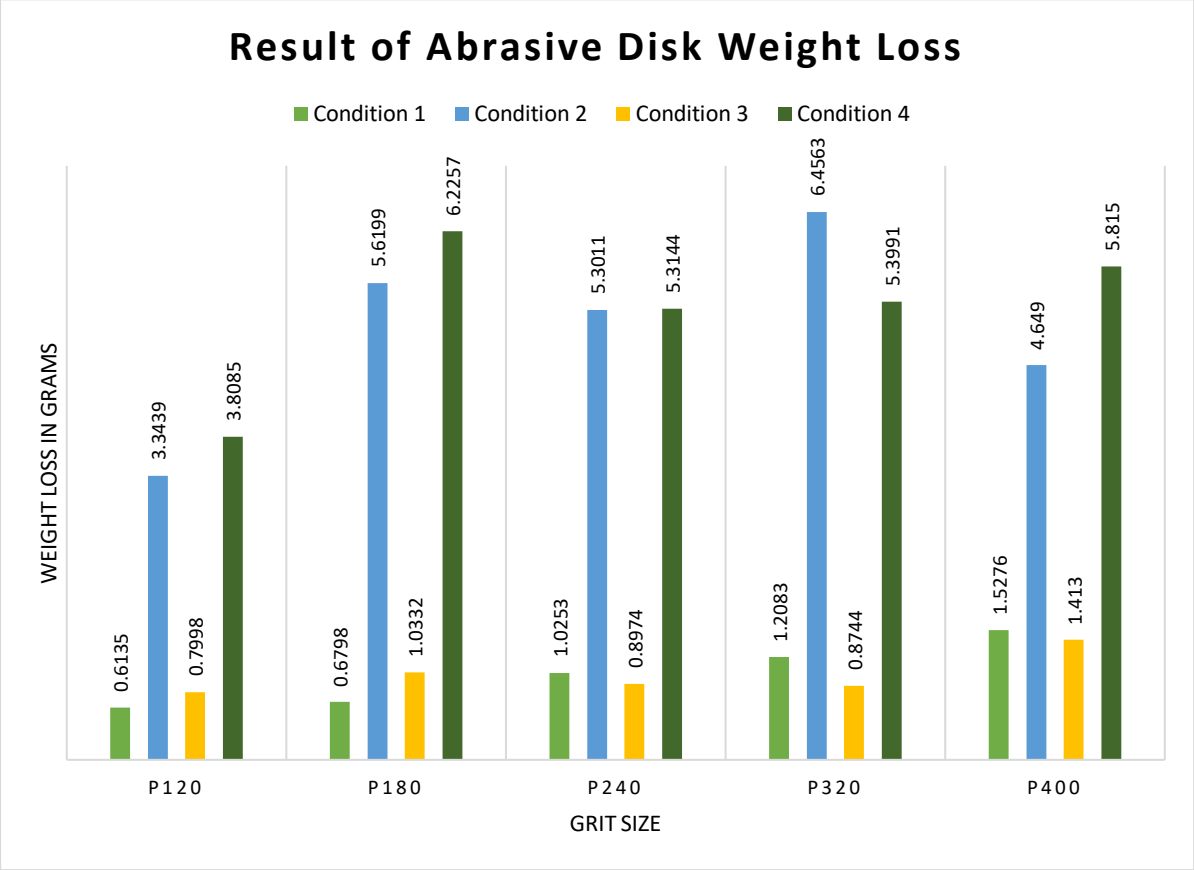

Figure 20. Abrasive disk life study by calculating the total weight loss after 9 minutes of random-orbital polishing.

Tool temperature during the random-orbital polishing is an important parameter as it influences the abrasive disk life. The known temperature of the abrasive disk is around 82°C by the existing method with the single-axis rotary tool. To further investigate the effects of relative temperature with the air and water medium for random-orbital polishing, temperature readings of the abrasive disk are taken to monitoring all conditions. In the preliminary stage, a portable infrared laser gun with a 12:1 distance to spot ratio capacity was used. This initial method of measurement detects the heat signature at a stand-off distance of approximately 20 mm. However, spot method is not accurate and it is challenging to use a single spot measurement across random locations on the abrasive disk area. Therefore, a forward-

looking infrared (FLIR) camera is used instead (figure 21). The average temperature of the random-orbital abrasive disk is recorded at 3-minute intervals from 0-9 minutes.

(21a) (21b) (21c)

Figure 21. Thermal images of the abrasive disk for (a) single-axis rotary tool, (b) random-orbital tool in condition 1, and (c) random-orbital tool in condition 4. All images are taken after 9 minutes polishing time. The yellow spectrum indicates a hot zone and blue is the colder region.

Figure 22 shows a summary of all the temperature readings from 0 to 9 minutes. From the experimental setup with the water- and air-cooling features (conditions 2 and 4), the polishing system is able to maintain or lower to a constant temperature in the 3- to 9-minute range. Compared with condition 1 (dry) that reached a peak temperature of 48.3°C (P120), condition 3 (cool air) exhibits a slower rate of temperature rise, except for P180 grit size, which saturates after the 4-minute mark. Overall, condition 4 (cool air and water) reaches the lowest temperature of 15.7 °C (P400) as compared with the other conditions due to higher efficiency of the air-cooled water medium.

This demonstration, when compared to the micrographs from figure 16 shows that with or without cooling medium employed (conditions 1 and 4), the microstructures preserve their properties with very limited thermal influence or degradation of the polished surface. The abrasive operation in condition 1 does not have any significant influence on the surface integrity because there is no evidence of white etching layer in comparison to the bulk material that could have resulted from plastic deformation by the heat and stresses generated.

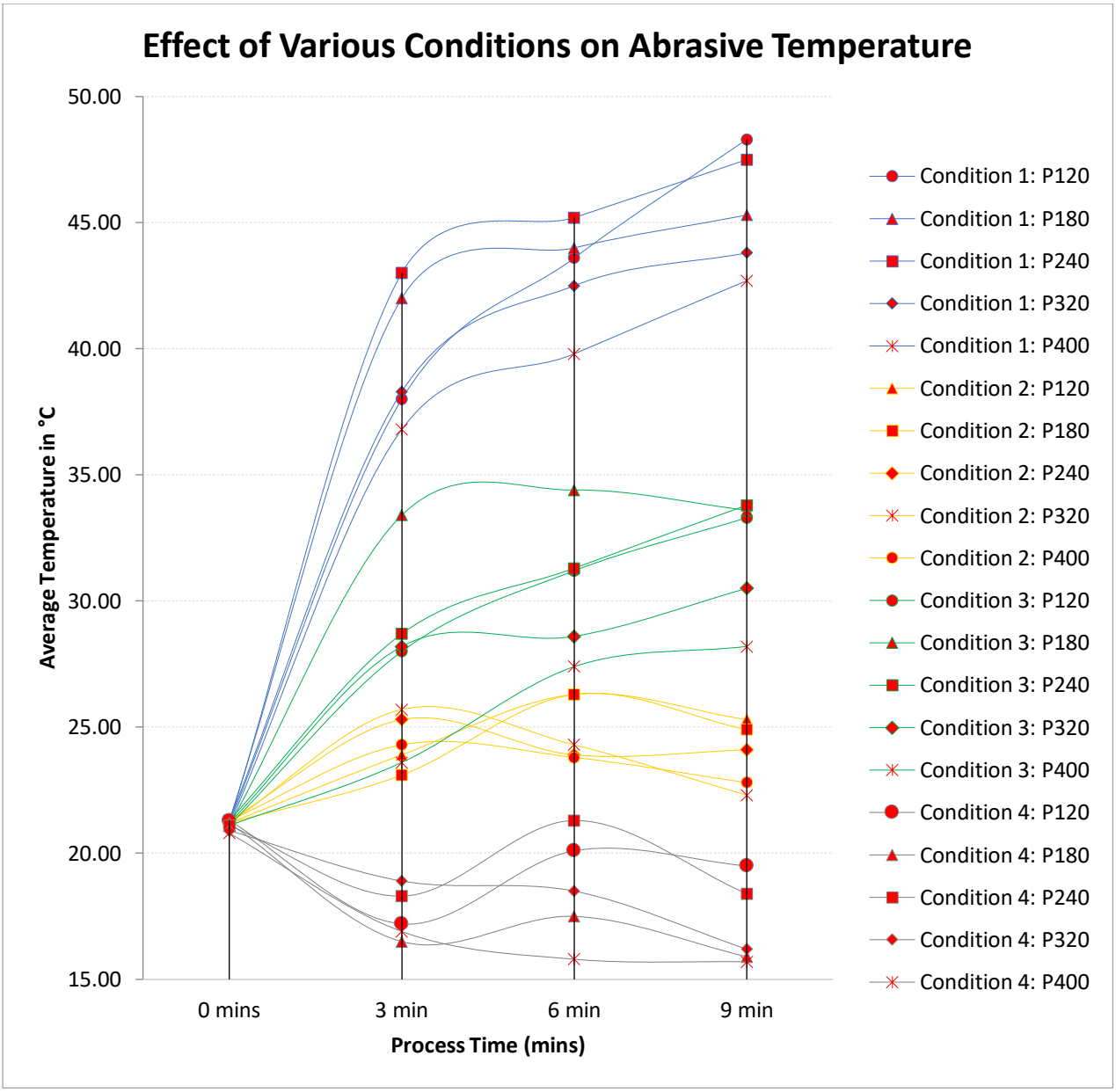

Figure 22. Average relative temperatures measured on the random-orbital abrasive disk at 3-minute intervals for a total of 9 minutes.

It is shown that the colloidal silica accumulated into a porous bulk structure, which is attributed to its high surface area as examined in microscopy.

3.4 Material removal and thickness measurement

The thickness of the polished sections of fan blade leading edge is measured using a digital dial indicator Mitutoyo 543-400B. The line markings are traced onto the fan blade surface and a cross-hair are drawn to intersect the lines at 25 mm distance from the leading edge of the fan blade (see Figure 23).

Figure 23. Thickness measurement of the leading edge with a digital dial caliper gauge

In order to remove the scallop height defects and retain the thickness dimension, the polishing method needs a lower material removal rate. Figure 24 shows the calculated cutting speed (*Vc*) for the four conditions by random-orbital polishing. The thickness of the specimen was measured before and after polishing and the data plotted on the graph for comparison.

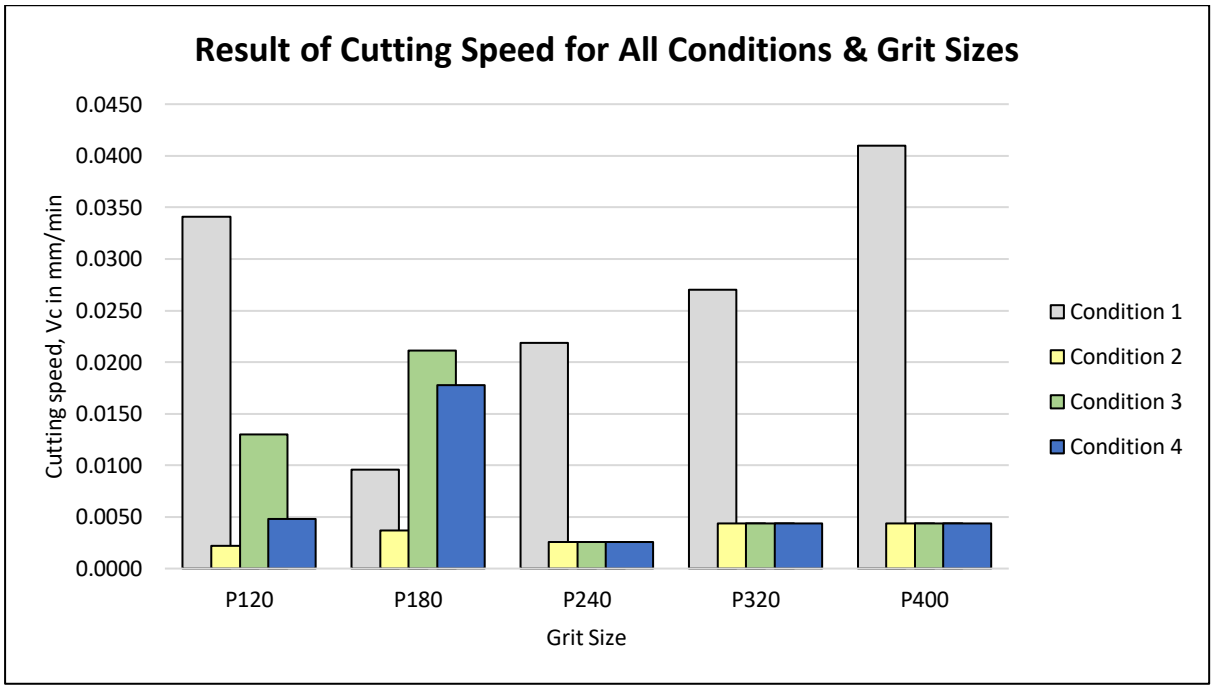

Figure 24. Random-orbital cutting speed (mm/min) calculated based on measuring the thickness height of the specimen before and after polishing for 9 minutes.

3.5 Overall comparison

Table 8 shows a summary of the comparative analyses of the new random-orbital method with varying experimental conditions and how they compared with the existing rotary polishing method. The results can be grouped into 3 classifications:

Group 1 (rotary polishing) – produced a matte surface with anisotropic finish (detrimental);

Group 2 (conditions 1 and 3) – produced a glossy surface with fine scratch marks in cross-hatched circular pattern (detrimental);

Group 3 (conditions 2 and 4) – produced a satin surface with isotropic non-directional finish and homogeneous (ideal).

Table 8. Summary of roughness and furrow for all processes from as-machined

Process	CNC Milling	Rotary Polishing	Random-Orbital Polishing	Random-Orbital Polishing	Random-Orbital Polishing	Random-Orbital Polishing
Condition	As-machined	Wet	Dry	Wet	Dry, Cold Air	Wet, Cold Air
Roughness parameters						
Ra (µm)	0.90	1.23	0.32	0.97	0.34	0.82
Rz (µm)	4.30	6.67	3.95	6.93	3.83	5.86
Sa (µm)	1.15	1.39	0.35	1.25	0.29	0.78
Sz (µm)	7.54	19.83	4.94	10.97	4.88	7.73
Furrow parameters						
Max. depth (µm)	4.94	17.64	3.89	9.18	3.98	5.85
Mean depth (µm)	2.14	3.42	0.69	2.34	0.56	1.51
Mean density (cm/cm^2)	903.12	1126.82	1124.72	1120.09	1125.91	1132.34

4.0 Conclusion

This paper demonstrates and evaluates the feasibility of a newly developed random-orbital tool categorized by four different conditions for localized polishing on fan blade leading edges. The post-polished surface texture of the specimens shows the process capability in removing scallop heights while keeping the edges within dimensional tolerance and producing the required roughness. Evaluation of the new method narrows the feasibility from four conditions to one recommendation: condition 4 (wet, cold air). Condition 4 performs the best in terms of achieving the target roughness and texture close to final finishing condition. The recommended method produces no microstructural defects and retains its harness close to nominal value. However, the disadvantage for this method is the shorter abrasive disk life after the polishing process, which may be slightly costlier in a high-volume production scenario.

Condition 1 (dry) is excluded in the down-selection because of the high abrasive temperatures, generation of dust and formaldehyde, creating a safety hazard to the operator. Furthermore, the surface topography (*Ra*) is beyond the desired target and there were visible scratch marks on the surface. Condition 2 is eliminated due to the significant drop in hardness and highest abrasive wear. Condition 3 is unsuitable because of gouging defect and uneven profile in the microstructure. In addition to this,

599 the surface topography (*Ra*) and scratches are similar to that of condition 1. The key findings can be
600 made in the following comments:

601 1. *Surface roughness and hardness*. Random-orbital polishing conditions 2 and 4 can produce the
602 desired surface roughness *Ra* 0.8 to 1.0 µm and maintain the threshold value of $Ra \leq 2$ µm. It was
603 axiomatic that conditions 1 and 3 have lower the peak-to-valley heights (*Sz*) by 75% as compared with
604 the existing single-axis rotary method. This reduction in height may not be beneficial for coating
605 adhesion in subsequent processing. However, conditions 2 and 4 has a *Sz* reduction of 45% and 61%
606 respectively as compared with the exiting method. Although the *Sz* value does not have a determined
607 target value, it is adequate to consider a certain amount of acceptable height which is close to the final
608 process. In this aspect, condition 4 is identified as the prime technique. The hardness of the workpiece
609 under conditions 1, 3 and 4 was similar to the initial condition before polishing. However, condition 2
610 is validated to have a 10% lower hardness after polishing with only deionized water. Thus, only
611 condition 2 fails the hardness test.

612 2. *Surface integrity and defects*. All conditions 1 through 4 have adequate ability to remove scallop
613 heights on the as-machined fan blade specimens. The thicknesses of the leading edges are all measured
614 and found within acceptable limits. Metallographic cross-sectioning proved that there was no surface
615 distortion, no strain lines and no abrasive particle embedment remained on the polished specimens.
616 However, metallurgical analysis showed that random-orbital polishing in condition 2 (wet) can lead to
617 gouging and uneven surfaces. Although condition 1 (dry) reached an elevated temperature of 43.8°C
618 after 9 minutes with P320 grit size, no significant surface degradation was observed in the metallurgical
619 analysis, except for the fine scratch marks observed.

620 3. *Abrasive life.* The wear condition of the abrasive disk is highest for conditions 2 and 4, and lowest
621 for conditions 1 and 3. The use of deionized water in conditions 2 and 4 is found to be the key contributor
622 to influence the wear behavior. It is concluded that abrasive disk for condition 4 is moistened, whereas
623 the abrasive disk for condition 2 is heavily wetted by the application of deionized water. As a result,
624 conditions 2 and 4 requires 5 times the number of abrasive disks as compared to conditions 1 and 3 for
625 the polishing work. The lower air temperatures generated by the cold gun for conditions 3 and 4 is not
626 observed to have any noticeable effect on the abrasives or slurry.

627 4. Condition 4 is found to be most favourable without any defects or dimensional issues. This also mean
628 that it takes less time and effort to treat the surface in subsequent processing. By replacing the existing
629 single-axis rotary method with random-orbital method (condition 4), the component surface is expected
630 to be more homogenous after the final processing stage. Based on the evaluation from this study, it is
631 recommended to use random-orbital polishing with deionized water and cold air for combined defect
632 removal and surface finishing. The key process variables are established to keep the abrasive disk cold
633 and moist during operation.

634

Consent to participate

This is to confirm all the authors have agreed to participate and have contributed in the content of the paper.

Edgar Jeevan Danaraj, Swee Hock Yeo

Credit author statement

We would like to declare the contributions made by the following authors:

1) Edgar J Danaraj - Development of the experimental methodology, collection and compiling of data, and manuscript preparation
2) Swee Hock Yeo – outline of manuscript, review, analyses and editing of manuscript.

Declaration of interests

☒ The authors declare that they have no known competing financial interests or personal relationships that could have appeared to influence the work reported in this paper.

☐The authors declare the following financial interests/personal relationships which may be considered as potential competing interests:

No competing interest

Funding

Nil

Availability of data and materials

Nil

References

1. Axinte DA, Kritmanorot M, Axinte M, Gindy NNZ (2005) Investigations on belt polishing of heat-resistant titanium alloys. J Mater Process Technol 166(3):398–404.

2. Xiao GJ, Huang Y (2016) Equivalent self-adaptive belt grinding for the real-R edge of an aero-engine precision-forged blade. Int J Adv Manuf Technol 83(9–12):1697–1706.

3. Wu, D., Wang, H., Zhang, K. et al. Research on flexible adaptive CNC polishing process and residual stress of blisk blade. Int J Adv Manuf Technol 103, 2495–2513 (2019).

4. Danyluk S., Ng S.H. (2013) Chemical Mechanical Polishing (CMP). In: Wang Q.J., Chung YW. (eds) Encyclopedia of Tribology. Springer, Boston, MA.

5. Nasoohi N, Hoorizad M, Tabatabaei SF. Effects of Wet and Dry Finishing and Polishing on Surface Roughness and Microhardness of Composite Resins. J Dent (Tehran). 2017 Mar;14(2) 69-75. PMID: 29104597; PMCID: PMC5662511.

6. Ho-Chieh Wong, Noritsugu Umehara, Koji Kato, the effect of surface roughness on friction of ceramics sliding in water, Wear, Volume 218, Issue 2, 1998, Pages 237-243, ISSN 0043-1648,

7. H.Z. Choi, S.W. Lee, H.D. Jeong, J. Mater. Proc. Technol. 111 (2001) 256.

8. Nguyen, T. & Zhang, L. (2003). An assessment of the applicability of cold air and oil mist in surface grinding. Journal of Materials Processing Technology. 140. 224-230. 10.1016/S0924-0136(03)00714-3.

9. Saberi, A. & Rahimi, A.R. & Parsa, H. & Ashrafijou, M. & Rabiei, Farshad. (2016). Improvement of surface grinding process performance of CK45 soft steel by minimum quantity lubrication (MQL) technique using compressed cold air jet from vortex tube. Journal of Cleaner Production. 131.

10. Sung-San Cho, Yong-Kyoon Ryu, Seung-Young Lee, Curved surface finishing with flexible abrasive tool, International Journal of Machine Tools and Manufacture, Volume 42, Issue 2, 2002, Pages 229-236, ISSN 0890-6955.

11. Axinte DA, Kwong J, Kong MC (2009) Workpiece surface integrity of Ti-6-4 heat-resistant alloy when employing different polishing methods. J Mater Process Technol 209:1843–1852.

12. Zhao T, Shi YY, Lin XJ, Duan JH, Sun PC, Zhang J (2014) Surface roughness prediction and parameters optimization in grinding and polishing process for IBR of aero-engine. Int J Adv Manuf Technol 74:653 663.

13. Xue, Yunpeng & Arjomandi, Maziar & Kelso, Richard. (2013). The working principle of a vortex tube. International Journal of Refrigeration. 36. 1730-1740. 10.1016/j.ijrefrig.2013.04.016.

14. Bedamati Nayak, N. Ramesh Babu, A mechanistic approach to predict the material removal rate in Ice Bonded Abrasive Polishing (IBAP), Procedia Manufacturing, Volume 48, 2020, Pages 302-310, ISSN 2351-9789.

15. C. Rathinasuriyan, A. Mystica, R. Sankar, V.S. Senthil Kumar, Experimental investigation of cooling medium on submerged friction stir processed AZ31 magnesium alloy, Materials Today: Proceedings, 2021, ISSN 2214-7853.

16. Fu, Guanghui, "Modeling of chemical mechanical polishing at multiple scales " (2002). Retrospective Theses and Dissertations. 995.

17. Oh S, Seok J. Modeling of chemical-mechanical polishing considering thermal coupling effects. Microelectron Eng 85(11): 2191–2201 (2008).

18. Tseng W T, Wang Y L. Re-examination of pressure and speed dependences of removal rate during chemicalmechanical polishing processes. J Electrochem Soc 144(2): L15–L17 (1997).

19. Zhao D W, He Y Y, Wang T Q, Lu X C, Luo J B. Effects of the polishing variables on the wafer-pad interfacial fluid pressure in chemical mechanical polishing of 12-inch wafer. J Electrochem Soc 159(3): H342–H348 (2012).

20. Luo J F, Dornfeld D A. Material removal mechanism in chemical mechanical polishing: theory and modeling. IEEE T Semiconduct M 14(2): 112–133 (2001).

Figures

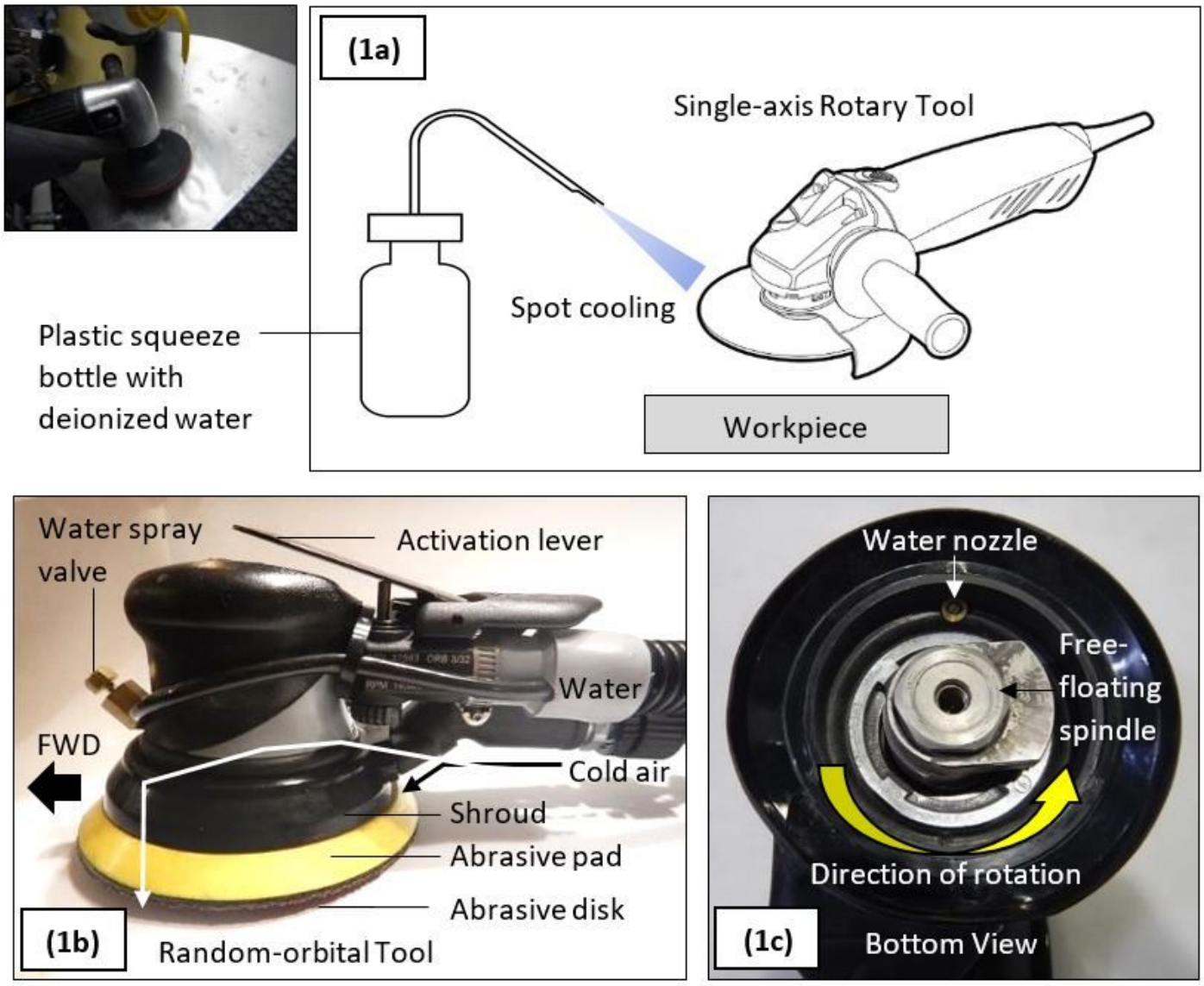

Figure 1

(a) Existing method by single-axis rotary tool with external spot cooling with a plastic bottled water, (b) Modified design of the random-orbital tool with integral cold air (indicated by the black arrow) and water (indicated by the white arrow), and (c) Free-floating spindle and water nozzle location (viewed from the bottom of the shroud with abrasive disk and pad removed).

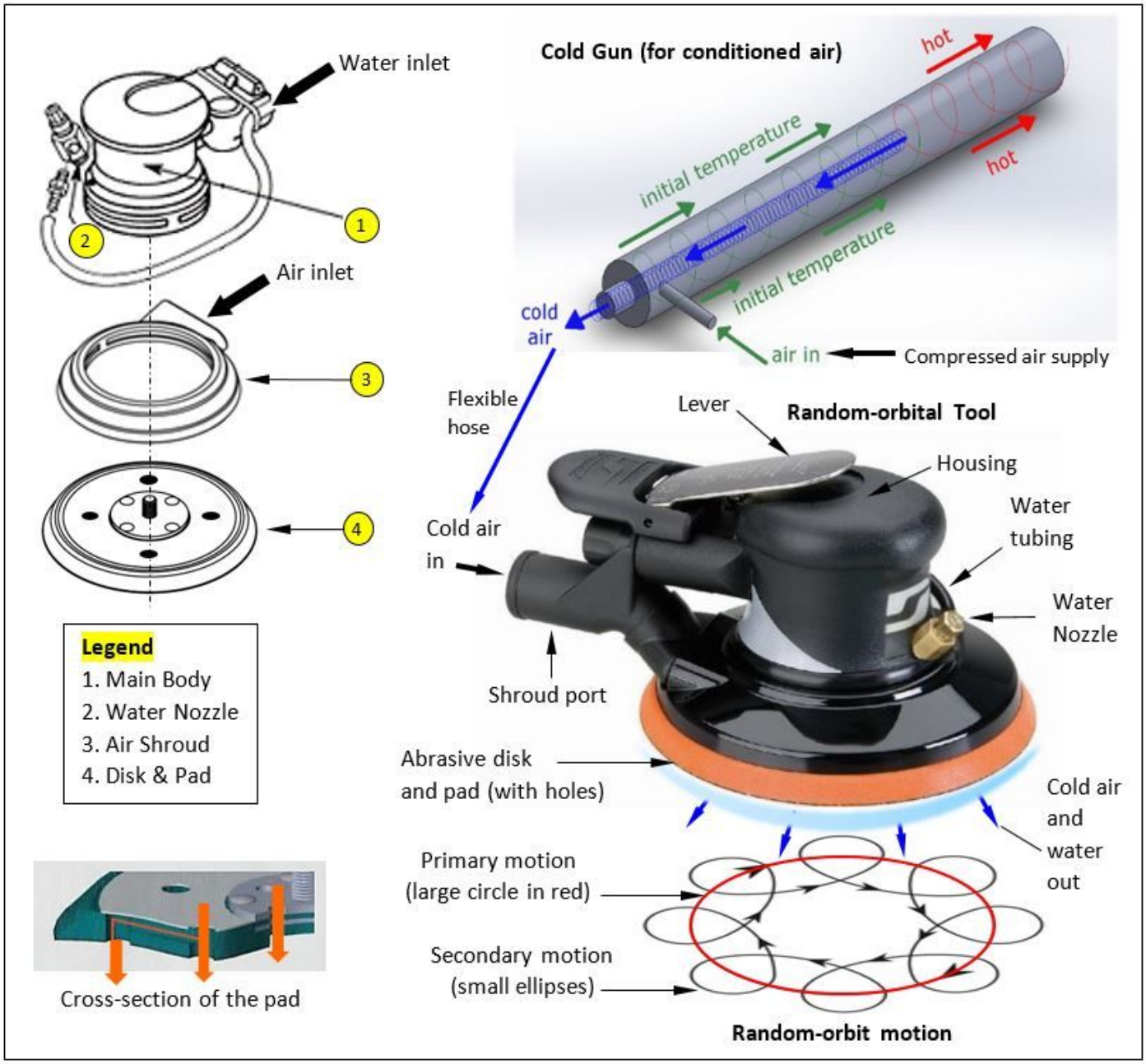

Figure 2

Schematic diagram of the main assembly components for the modified random-orbital tool showing the principle operation of the cold gun and the random-orbit motion of the tool path.

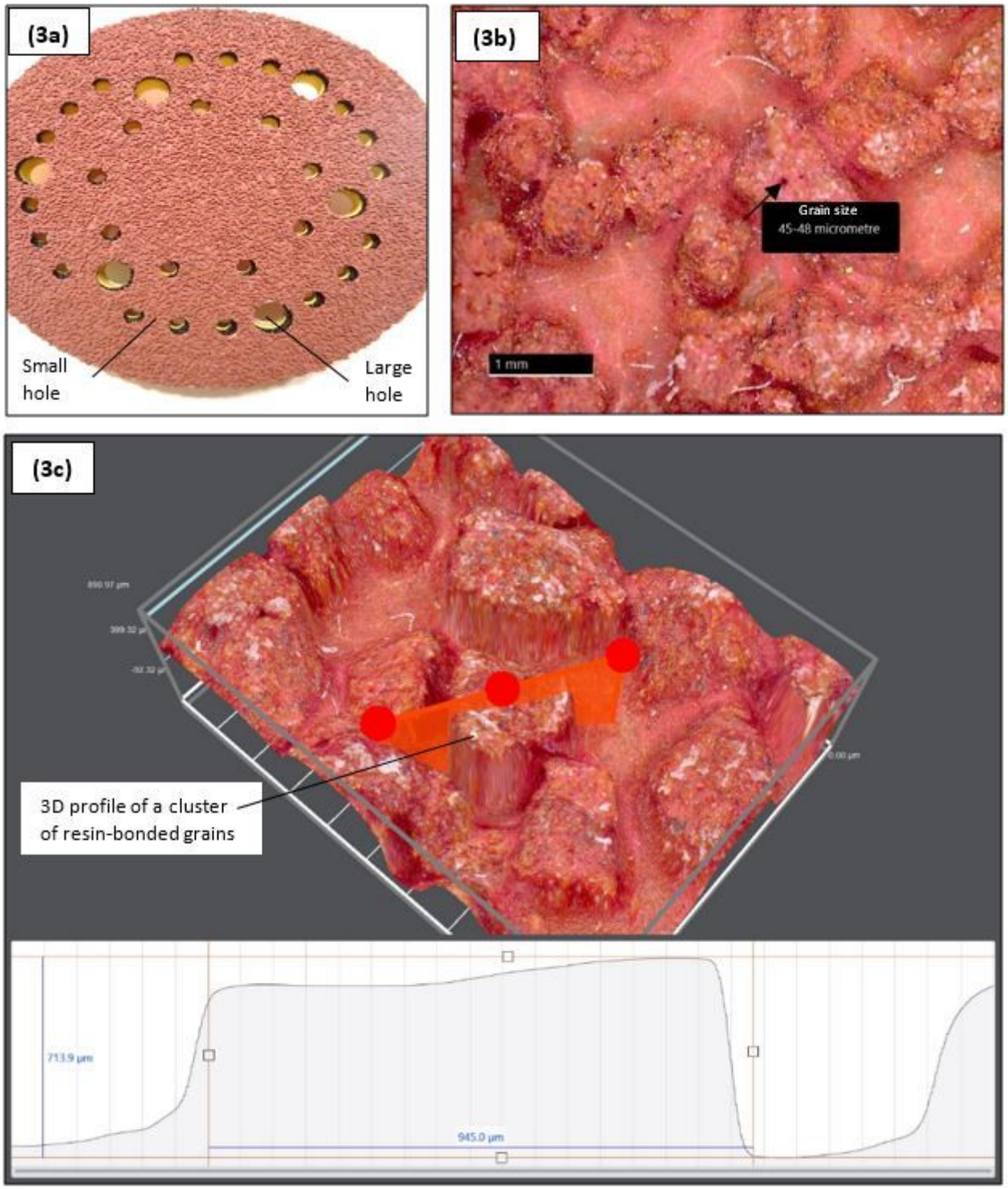

Figure 3

(a) Random-orbital tool with the customized hole pattern in the bonded abrasive disk and backing foam pad to form a matched set, (b) 2D section of an agglomerated abrasive structure of P320 grit. A grain size of P320 grit varied between 45 µm to 48 µm and (c) 3D cross-section of a P320 grit size aggregate showing typical dimensions of 713.9 µm in height and 945 µm in width.

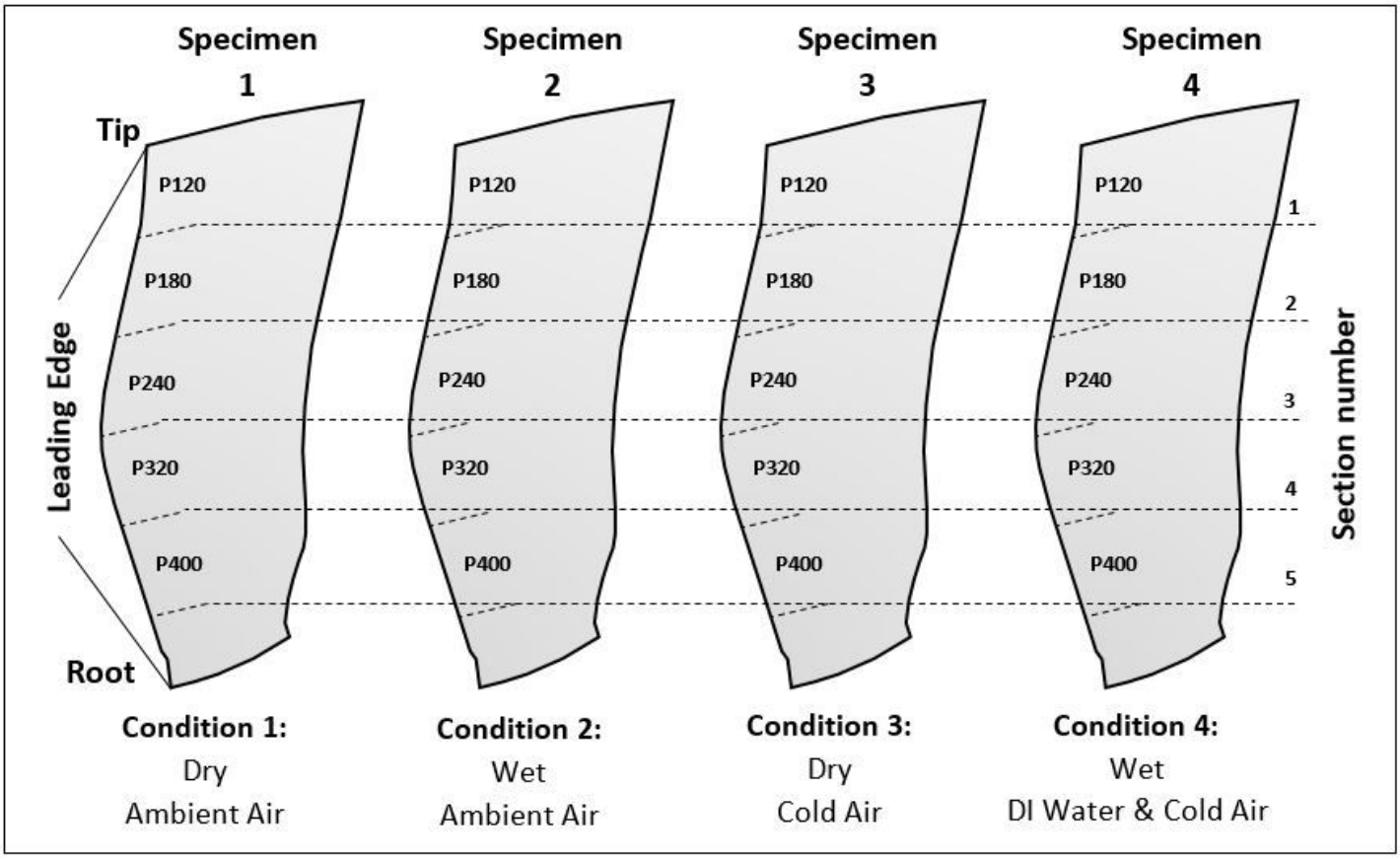

Figure 4

Experimental conditions of 4 aluminum alloy fan blade specimens (7255-T7751) with 5 different grit sizes. The target areas to be finished are at the leading-edge sections, from tip to root demarcated by the section numbers from the dotted lines (Grit sizes P120, P180, P240, P320 and P400).

Figure 5

(a) Polishing operation on the specimen, (b) basic components of the cold gun and (c) preliminary testing of the typical load applied on the part and (d) determining the highest load where the tool stops rotating.

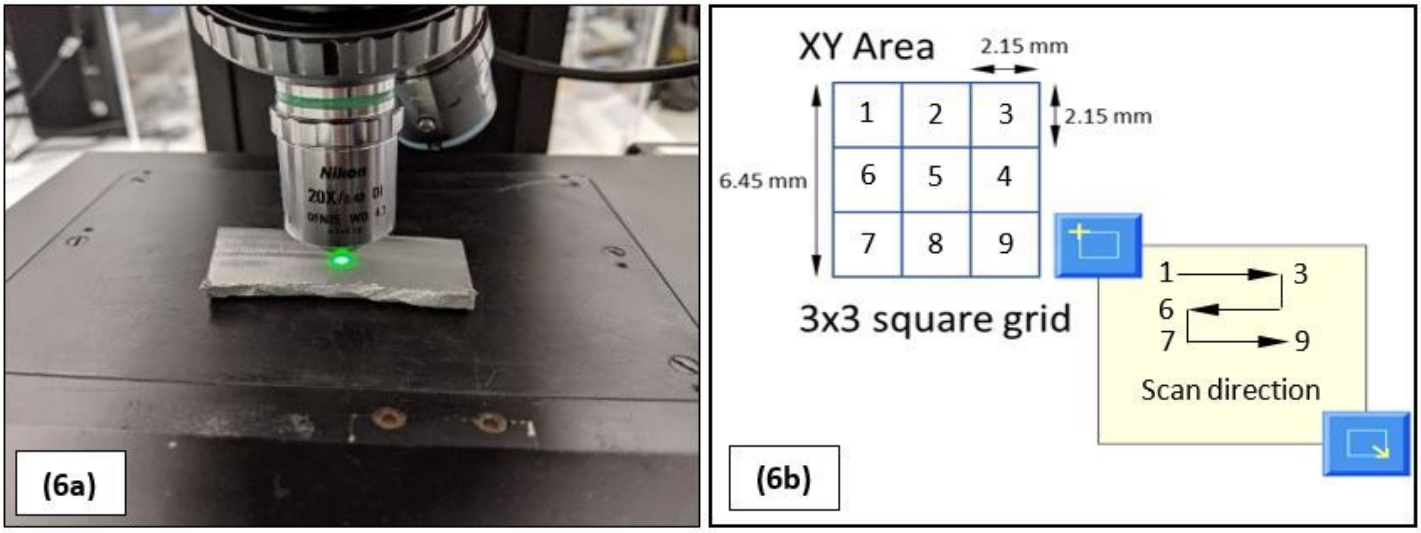

Figure 6

(a) CCI measurement on sample, and (b) X-Y scanning area and direction.

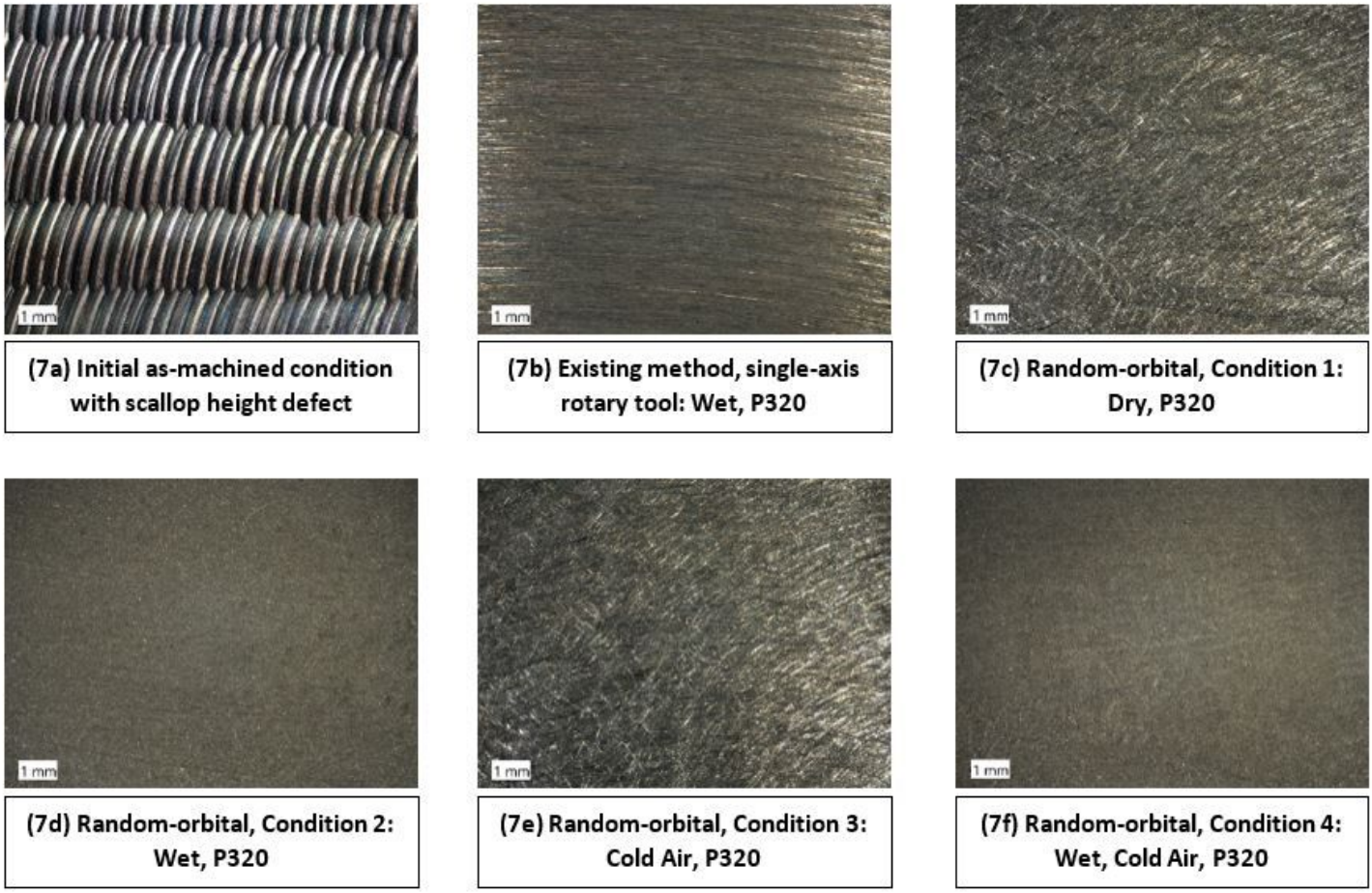

Figure 7

Images before and after polishing for 9 minutes with P320 grit size: (a) Initial, as-machined condition with scallop height defect, (b) Existing polishing method with single-axis rotary tool, wet condition, (c) Random-orbital method, condition 1; dry, (d) Random-orbital method, condition 2; wet, (e) Random-orbital method, condition 3; cold air, (f) Random-orbital method, condition 4; wet, cold air.

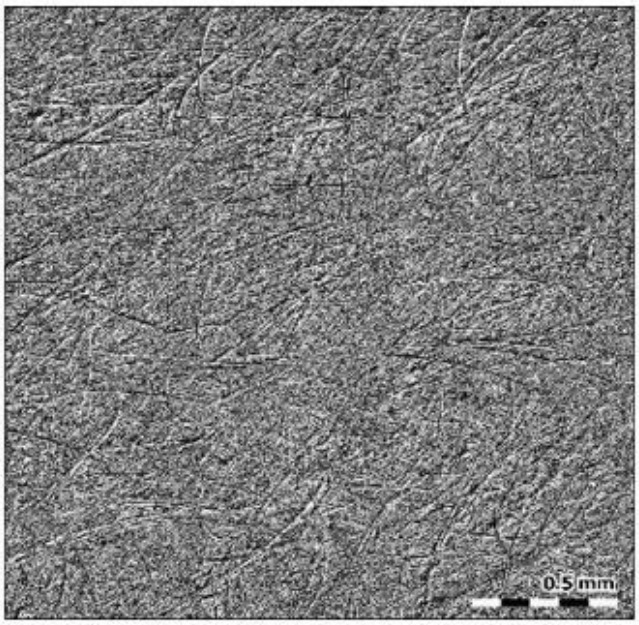

(8a) Random-orbital, Condition 1: Dry, P320 grit

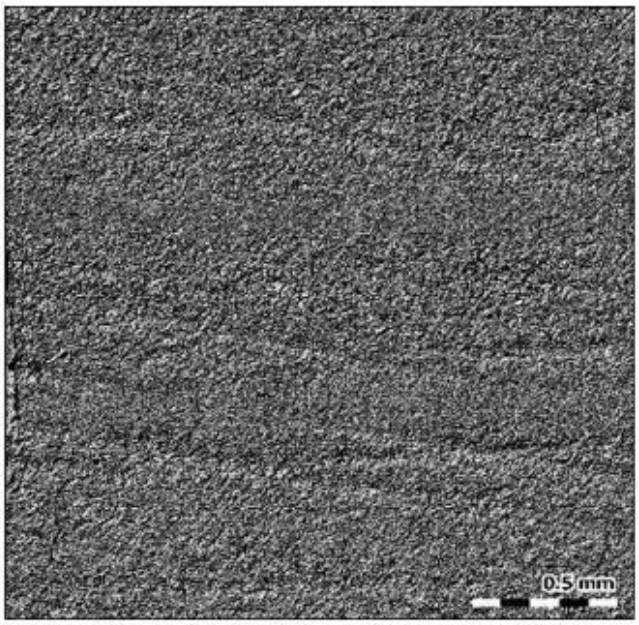

(8b) Random-orbital, Condition 2: Wet, P320 grit

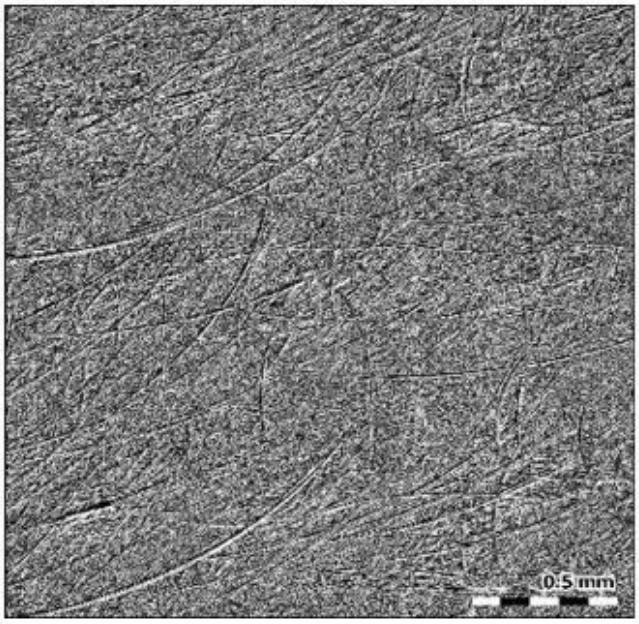

(8c) Random-orbital, Condition 3: Cold Air, P320 grit

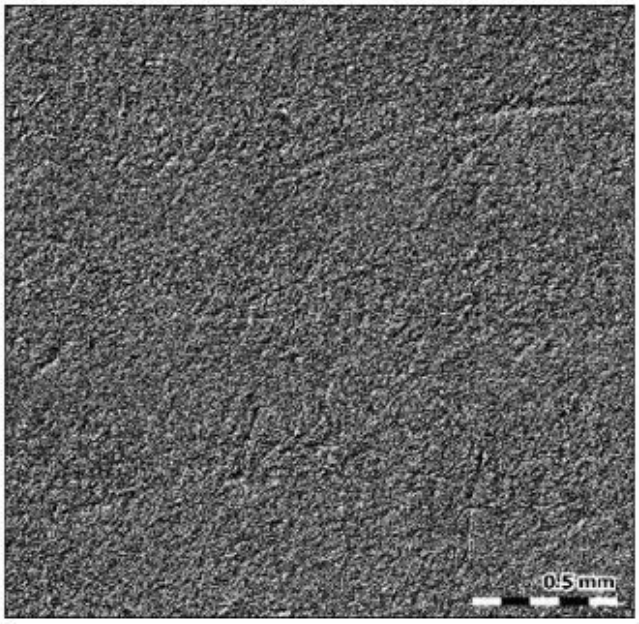

(8d) Random-orbital, Condition 4: Wet, Cold Air, P320 grit

Figure 8

2D surface topography comparison after random-orbital polishing for 9 minutes with P320 grit size: (a) Condition 1; dry, (b) Condition 2; wet, (c) Condition 3; cold air, (d) Condition 4; wet, cold air. Measurement instrument used was Talysurf CCI 3000.

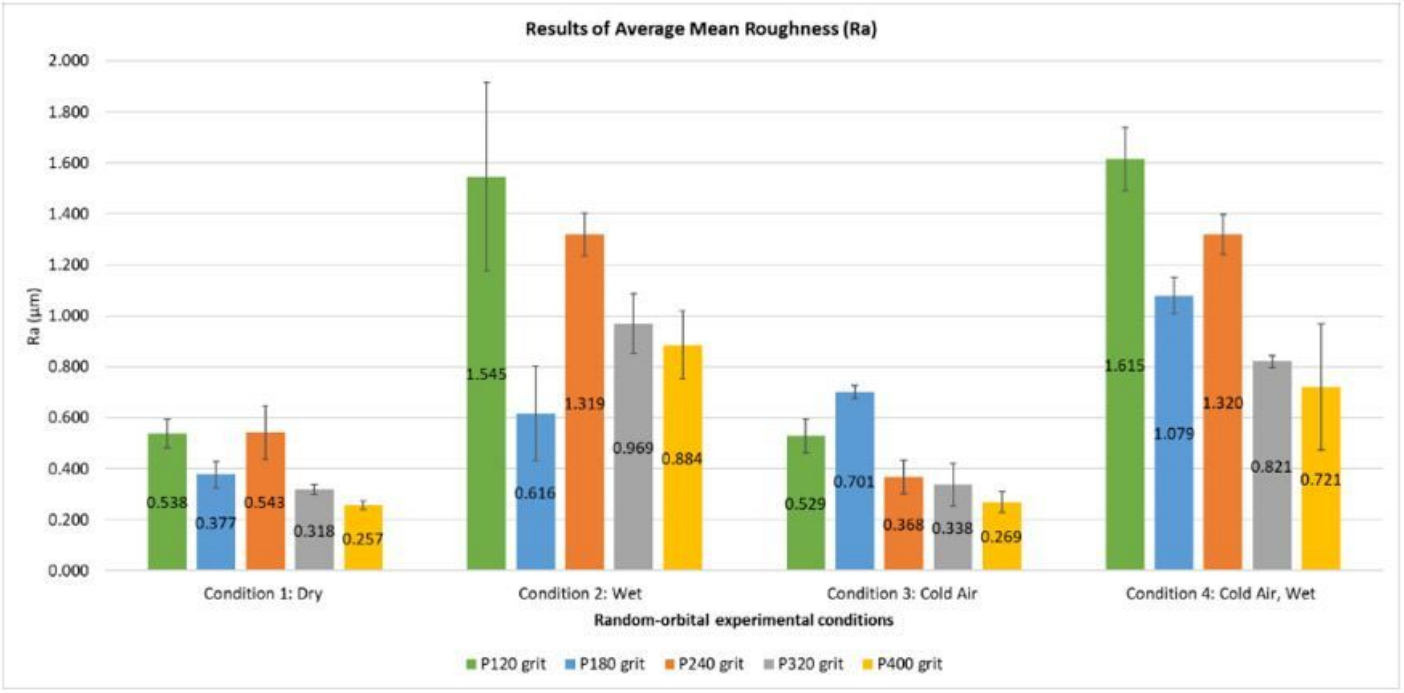

Figure 9

Results of Ra for all conditions with P120, P180, P240, P320 and P400 abrasive grit sizes. (Measurement instrument used was Talysurf CCI 3000).

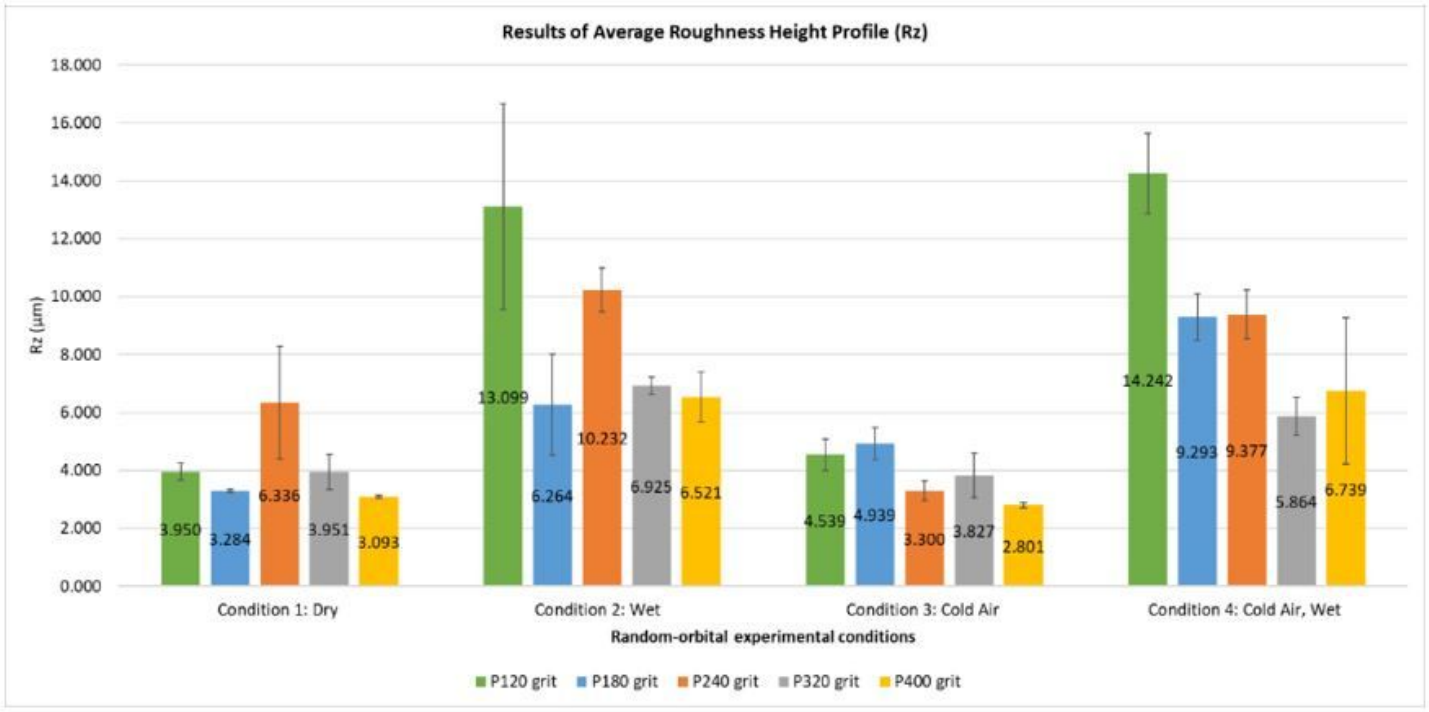

Figure 10

Results of maximum height profile (Rz parameter) for all conditions with P120, P180, P240, P320 and P400 abrasive grit sizes. Measurement instrument used was Talysurf CCI 3000.

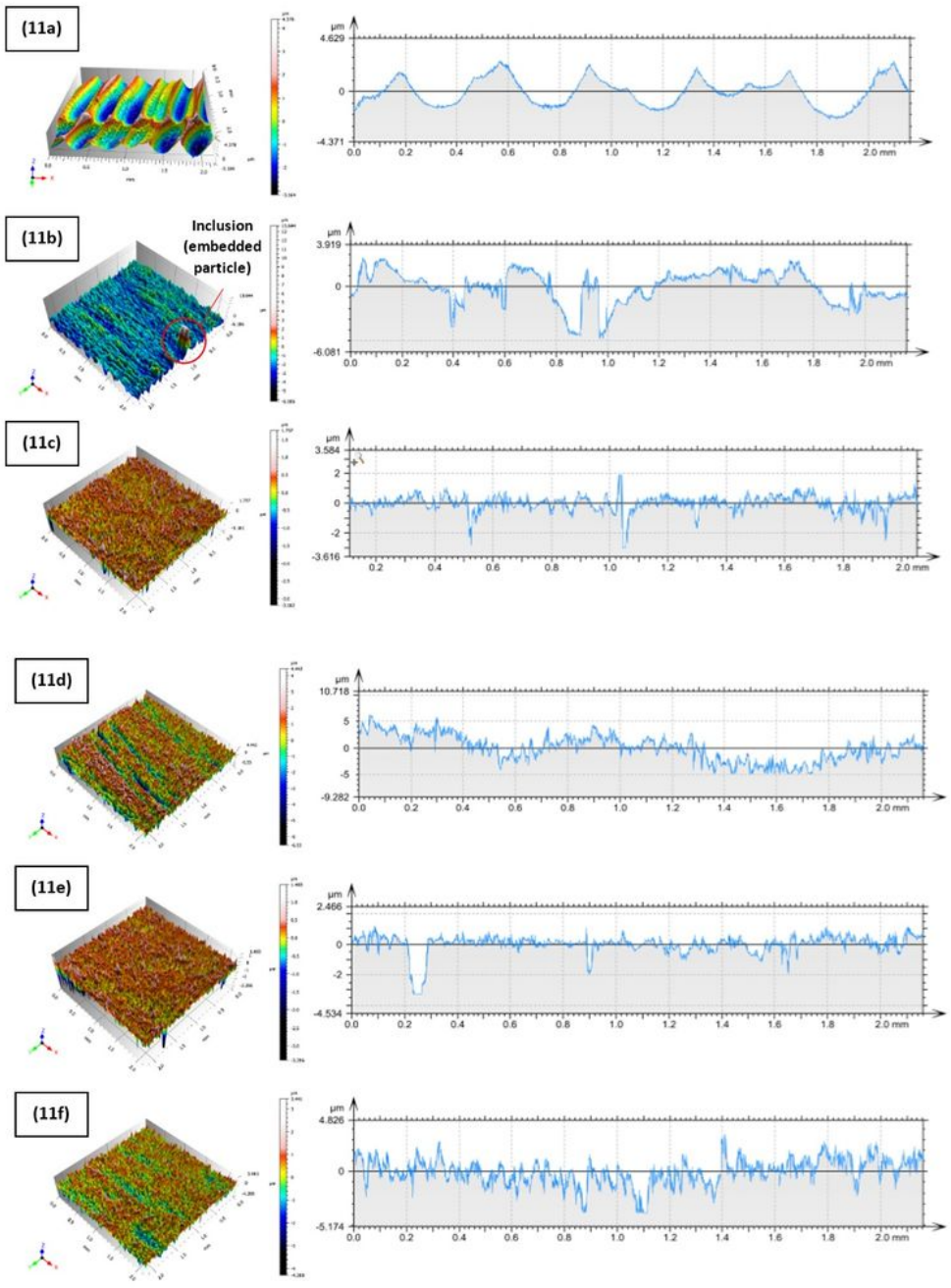

Figure 11

Surface profiles showing peak and valley by coherence correlation interferometry (CCI): (a) Initial, as-machined condition with scallop height defect, (b) Single rotary axis, wet, P320, (c) Random-orbital method, condition 1; dry, P320 (d) Random-orbital method, condition 2; wet, P320 (e) Random-orbital method, condition 3; cold air, P320, (f) Random-orbital method, condition 4; wet, cold air, P320. Measurement instrument used was Talysurf CCI 3000.

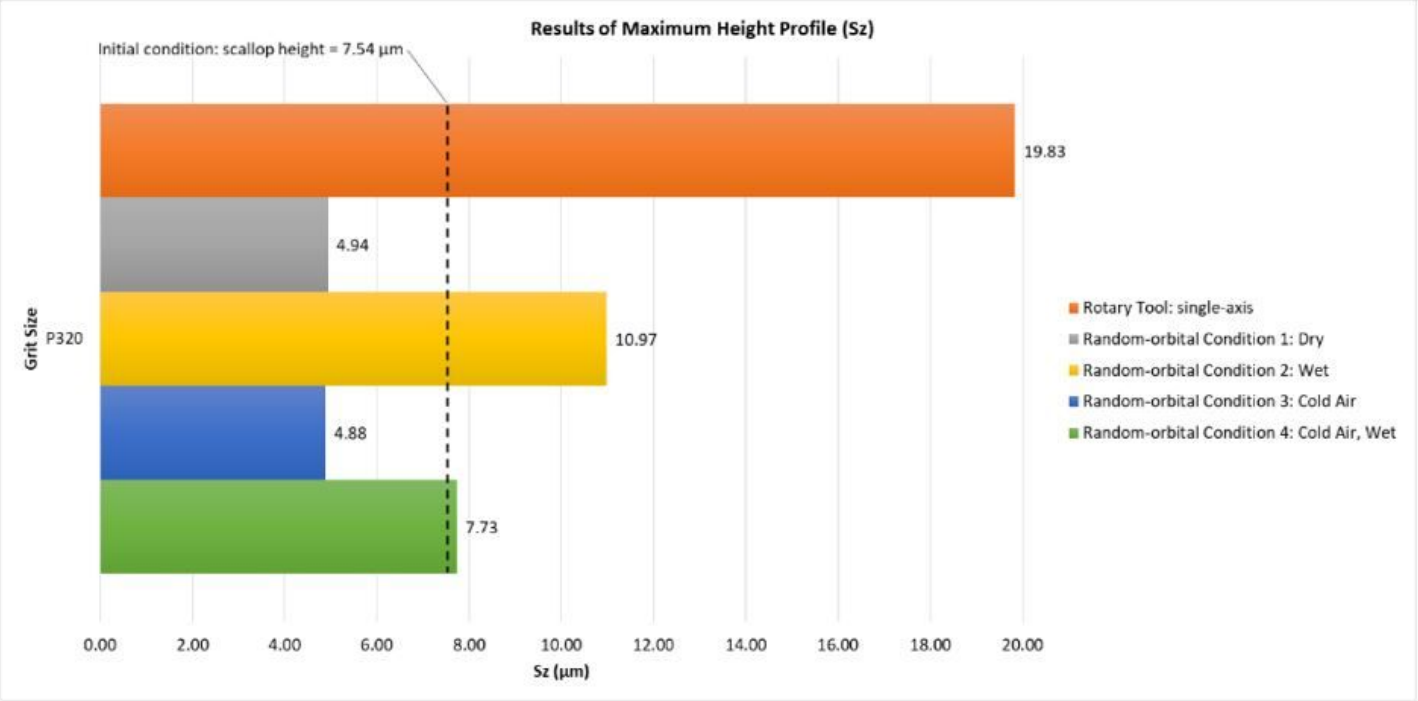

Figure 12

Results of maximum height profile (Sz parameter) for all conditions with P320 abrasive grit sizes. Measurement instrument used was Talysurf CCI 3000.

Figure 13

Results of average mean roughness (Sa parameter) for all conditions with P120, P180, P240, P320 and P400 abrasive grit sizes. Measurement instrument used was Talysurf CCI 3000.3.2

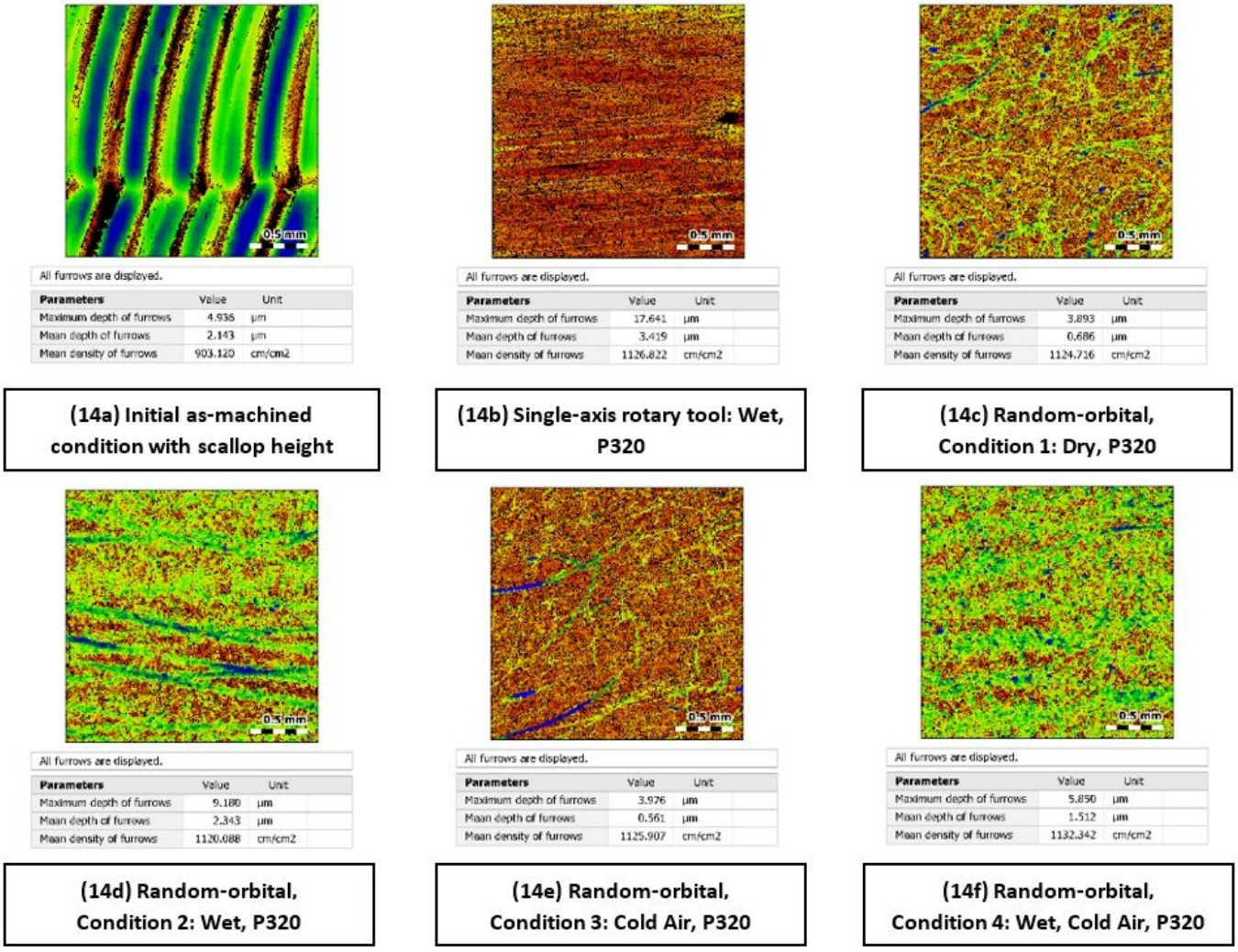

Figure 14

3D image and parametric report of furrows by coherence correlation interferometry (CCI) after polishing for 9 minutes with P320 grit size: (a) Initial, as-machined condition with inherent step mark defect, (b) Single rotary axis, wet condition, (c) Random-orbital method, condition 1; dry, (d) Random-orbital method, condition 2; wet, (e) Random-orbital method, condition 3; cold air, (f) Random-orbital method, condition 4; wet, cold air.

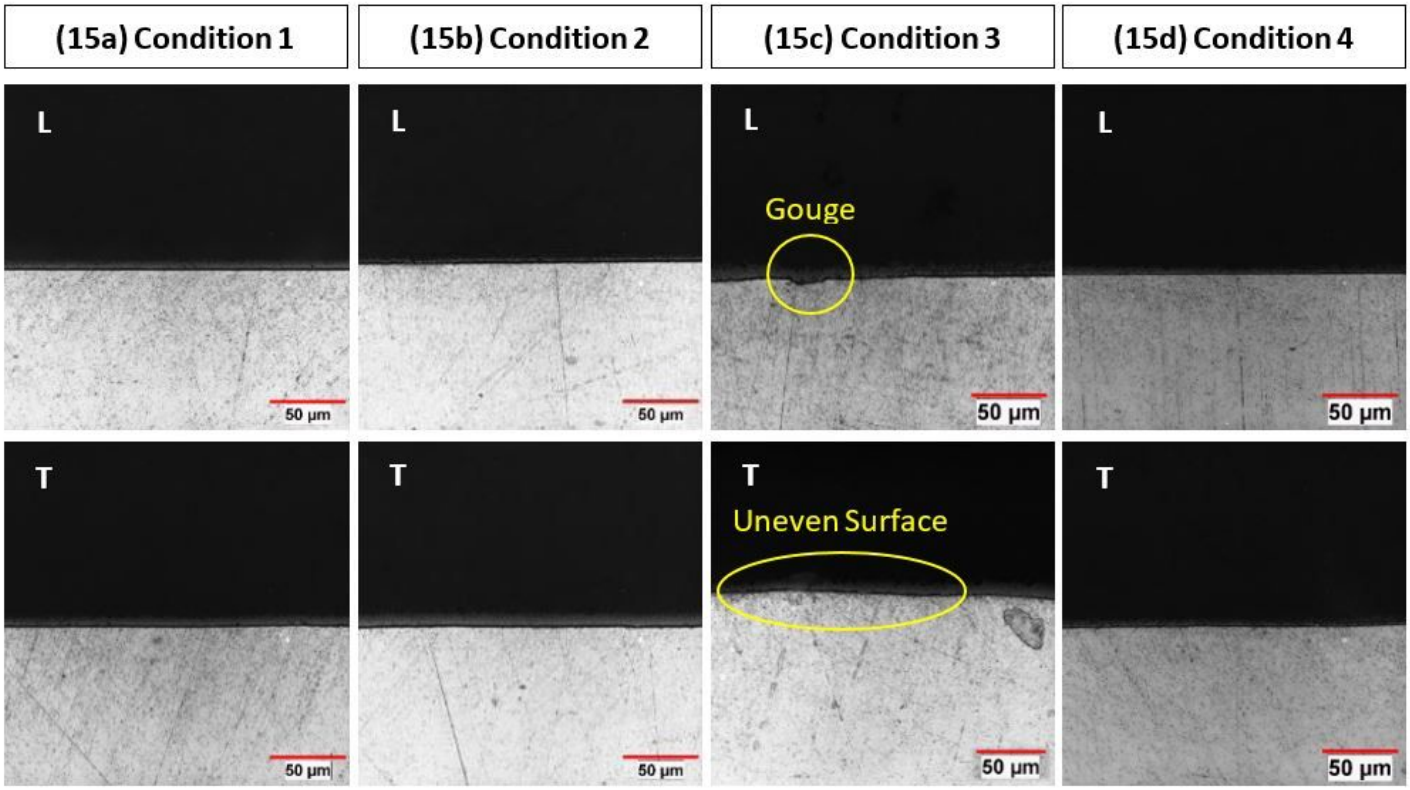

Figure 15

(a) to (d) Conditions 1 to 4: Microstructure of the random-orbital polished specimens with P320 grit size – lateral (L) and transverse (T) direction

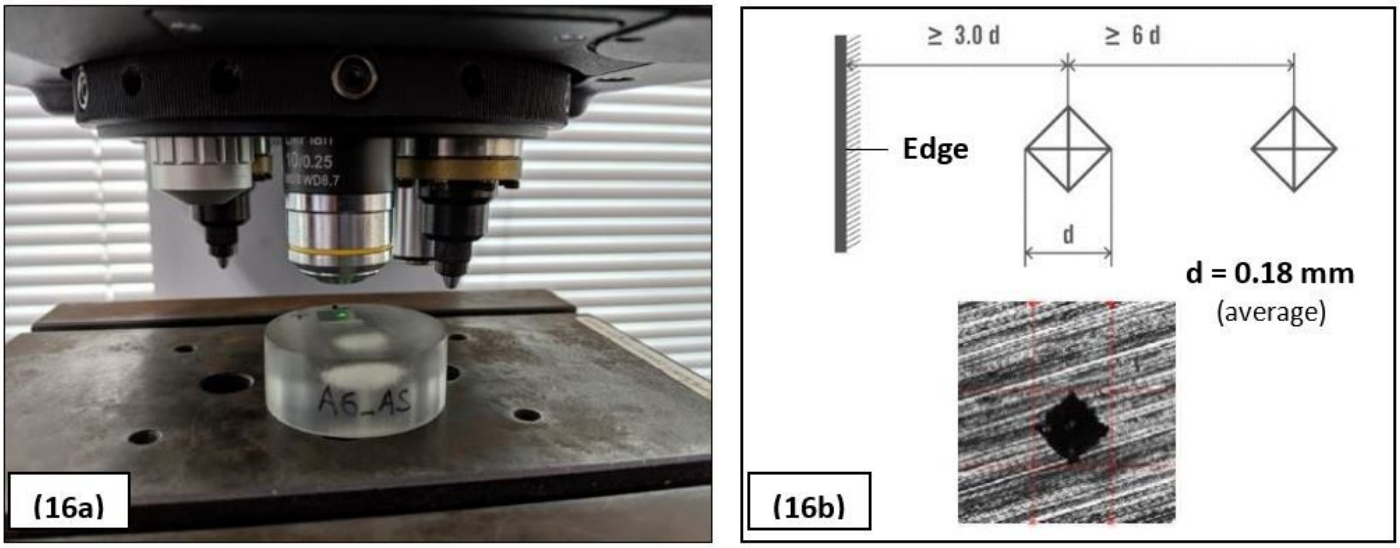

Figure 16

(a) Vickers hardness tester with sample mount and (b) indentation strategy on the sample surface (average of 3 readings taken)

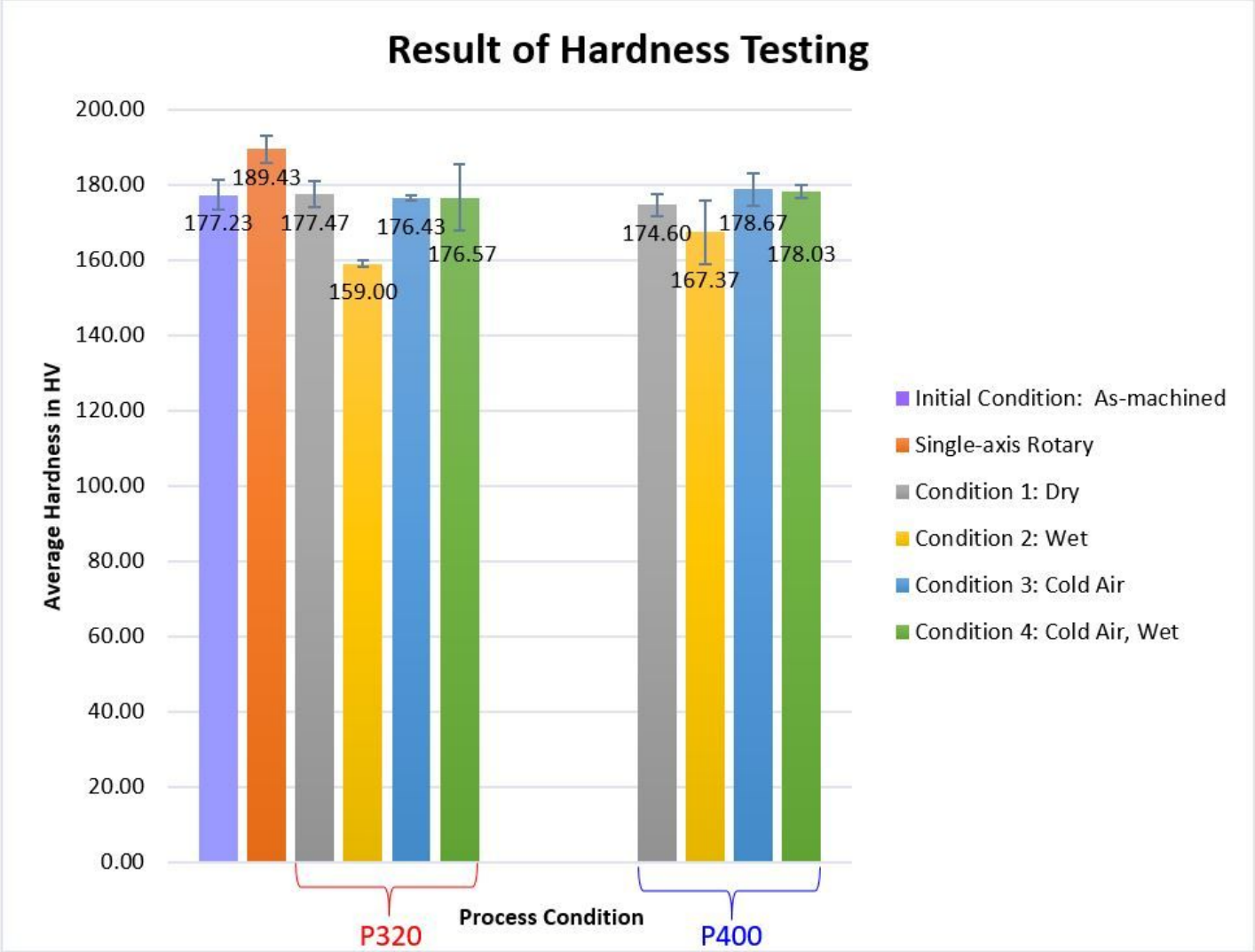

Figure 17

Micro-hardness test result for P320 grit size polished samples - average of 3 indentations for each condition carried out.

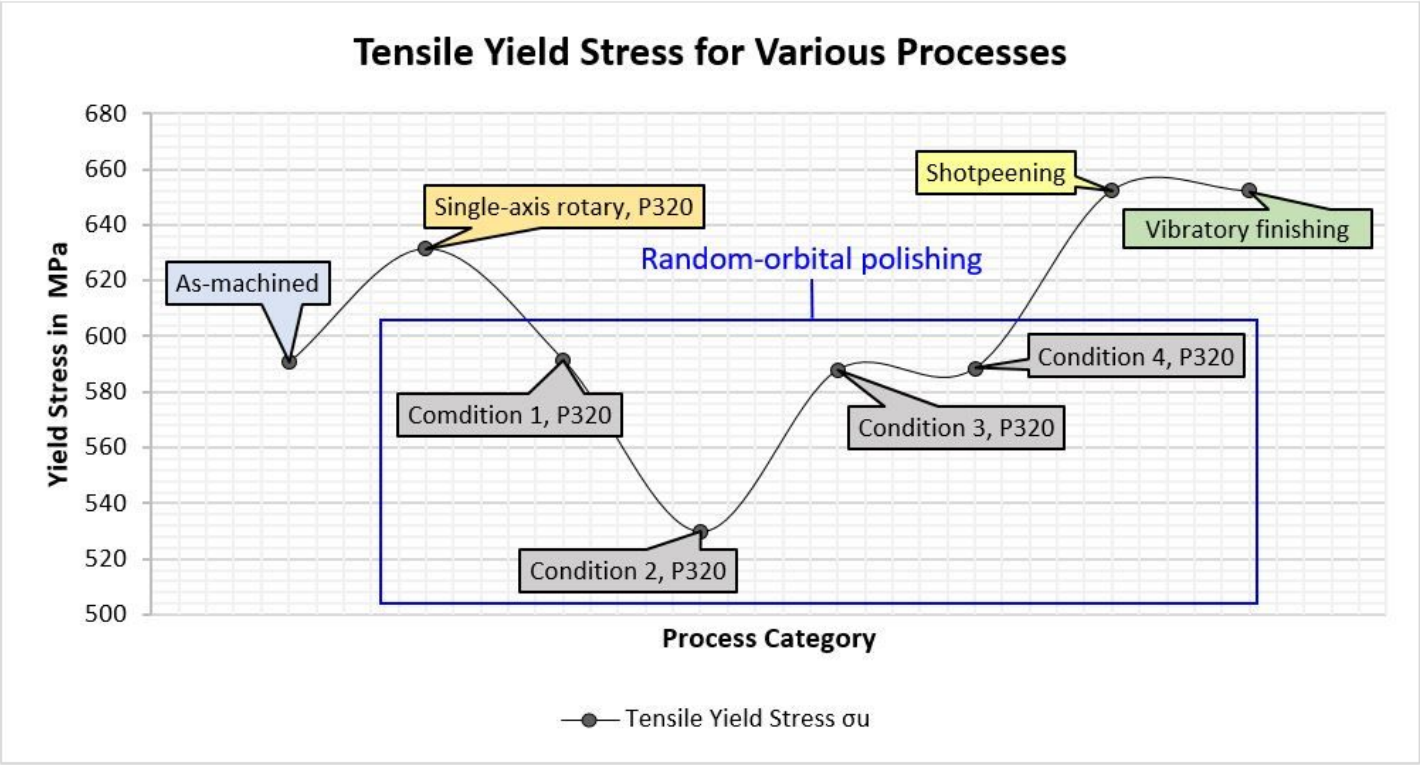

Figure 18

Approximate tensile yield stress calculated based on average hardness values.

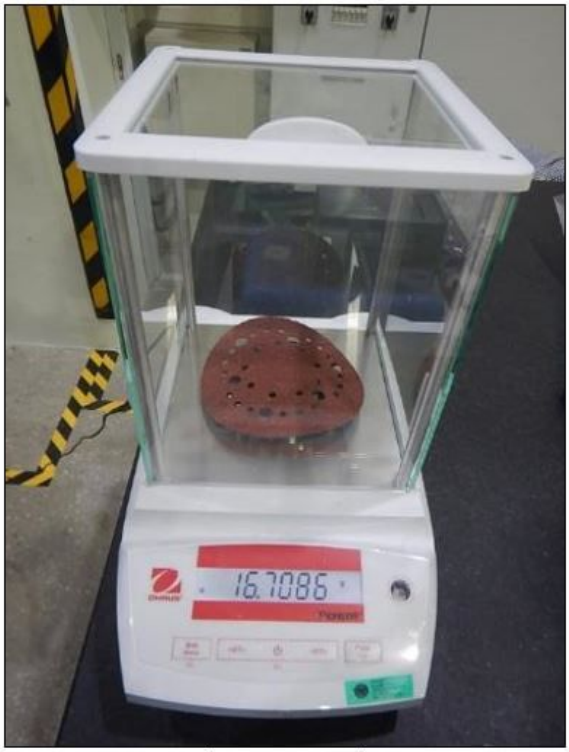

(19a)

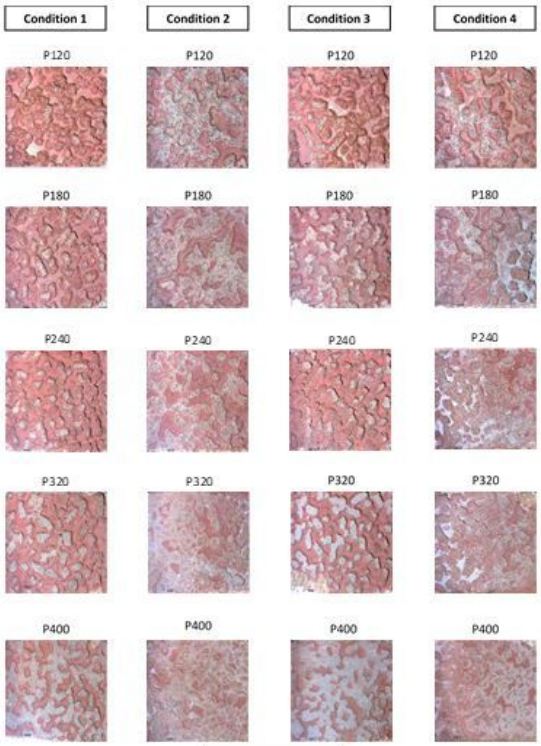

(19b)

Figure 19

(a) Abrasive disk is weighed before and after random-orbital polishing, and (b) abrasive disk samples inspected by digital microscope after 9 minutes of random-orbital polishing.

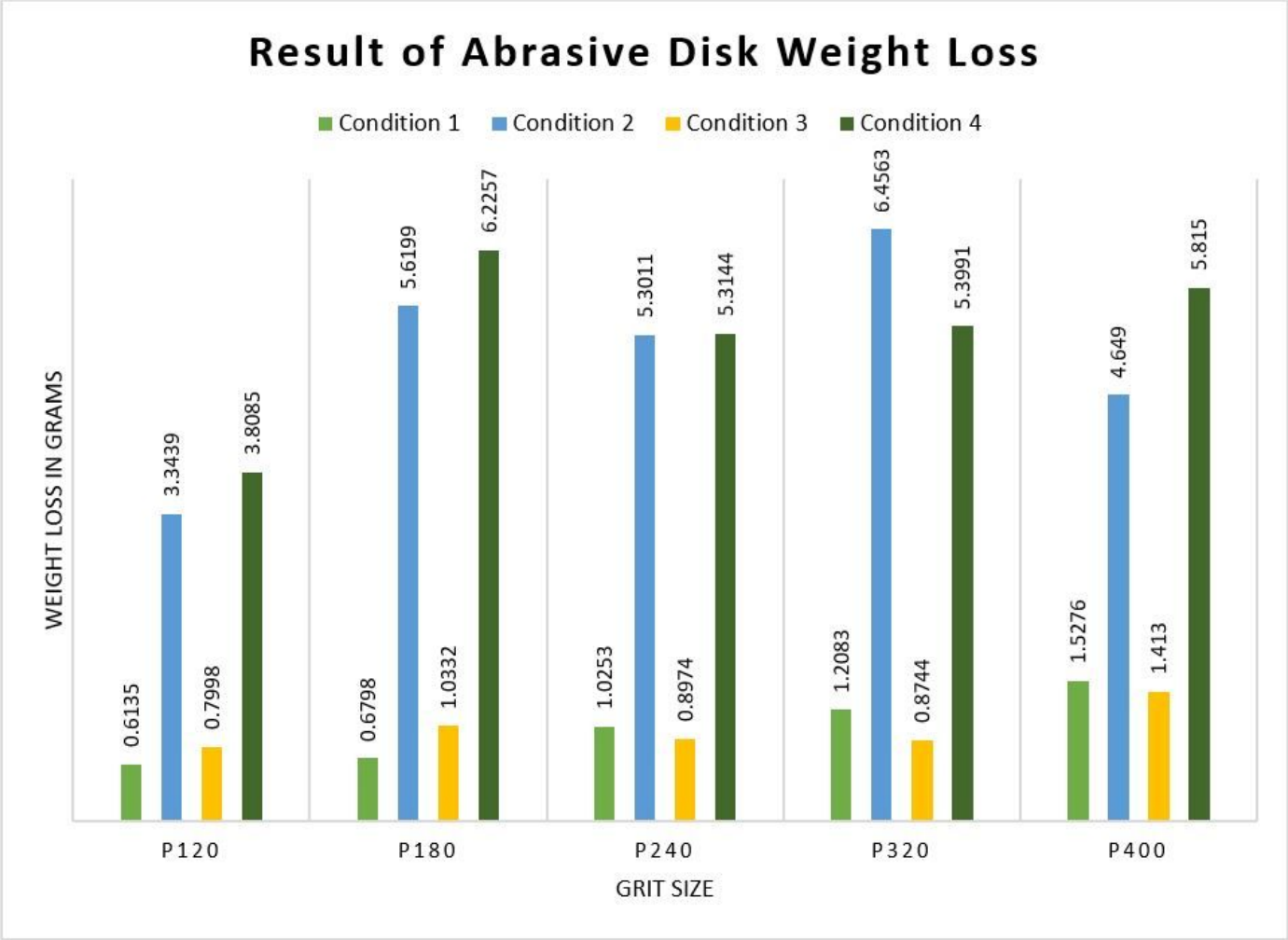

Figure 20

Abrasive disk life study by calculating the total weight loss after 9 minutes of random-orbital polishing.

Figure 21

Thermal images of the abrasive disk for (a) single-axis rotary tool, (b) random-orbital tool in condition 1, and (c) random-orbital tool in condition 4. All images are taken after 9 minutes polishing time. The yellow spectrum indicates a hot zone and blue is the colder region.

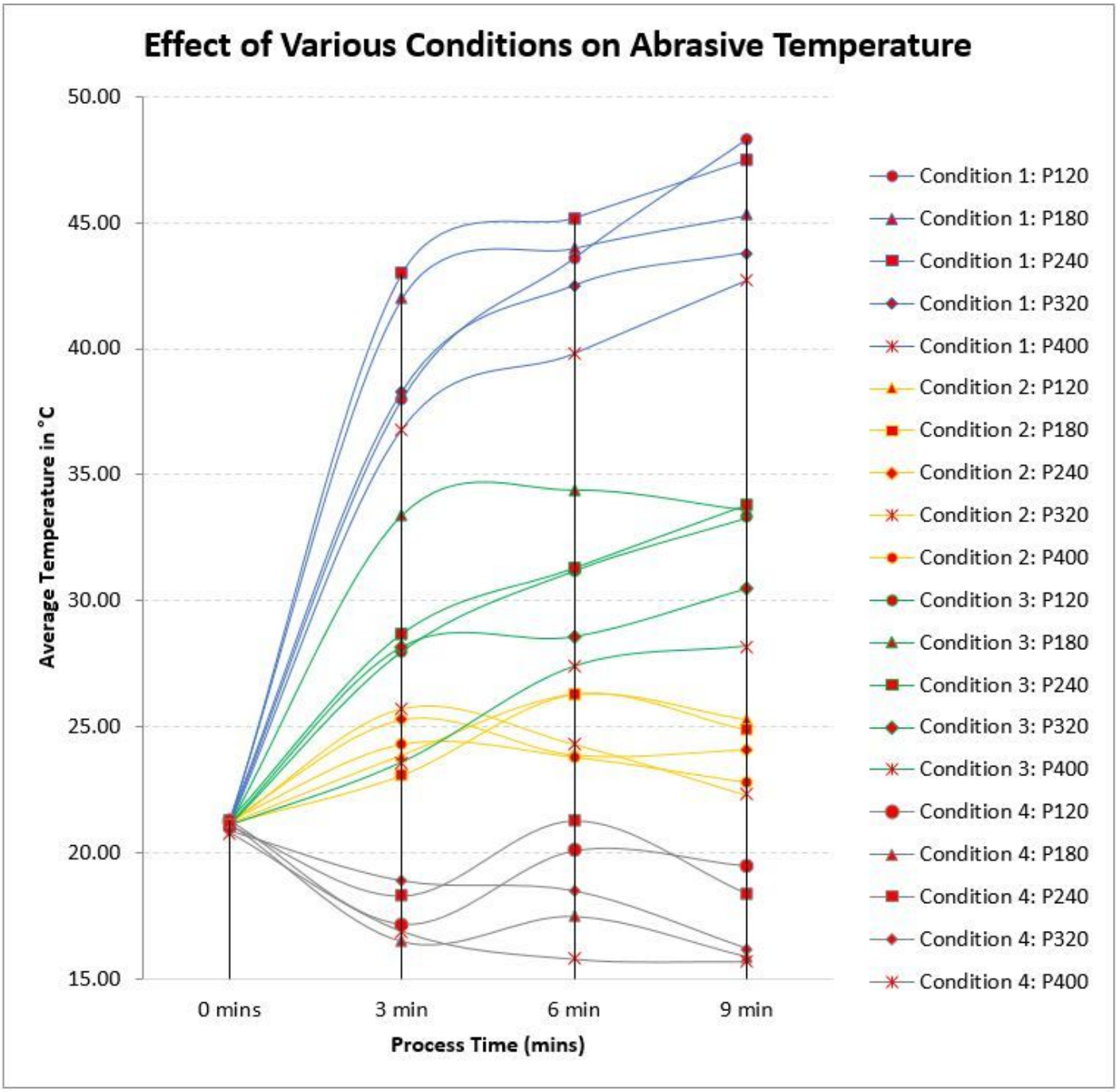

Figure 22

Average relative temperatures measured on the random-orbital abrasive disk at 3-minute intervals for a total of 9 minutes.

Figure 23

Thickness measurement of the leading edge with a digital dial caliper gauge

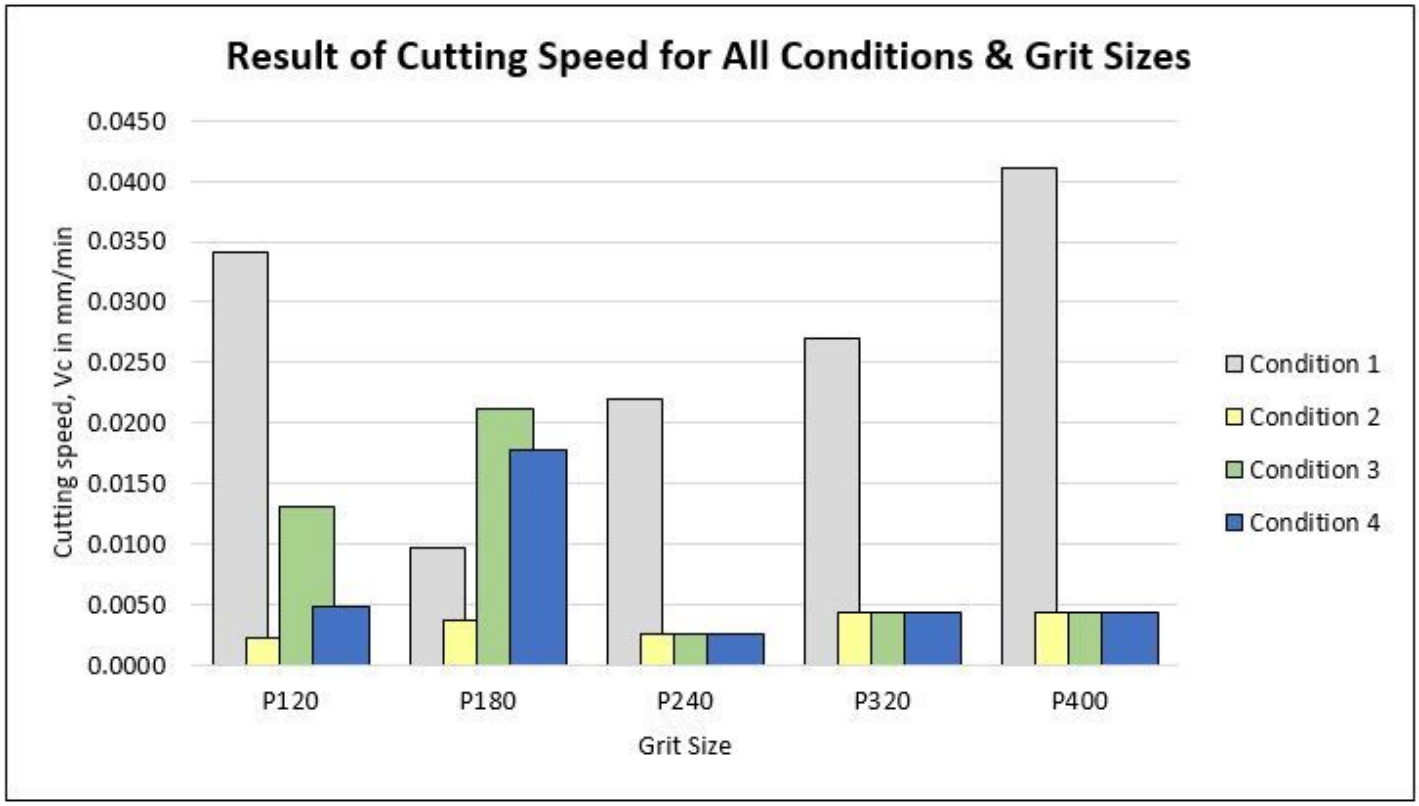

Figure 24

Random-orbital cutting speed (mm/min) calculated based on measuring the thickness height of the specimen before and after polishing for 9 minutes.